Auroral alert version 1.0: Two-step automatic detection of sudden auroral intensification from all-sky JPEG images

Masatoshi Yamauchi and Urban Brändström

Swedish Institute of Space Physics, Bengt Hultqvist vägen 1, Box 812, S-98128 Kiruna, Sweden

Correspondence: M. Yamauchi (M.Yamauchi@irf.se)

Abstract. Sudden and significant intensification of auroral arc with expanding motion (we call it "Local-Arc-Breaking" hereafter) is an important event in many aspects but easy to miss for real-time watching due to its short rise time. To ease this problem, a real-time alert system of Local-Arc-Breaking was developed for Kiruna all-sky camera (ASC) using ASC Joint Photographic Expert Group (JPEG) images. The identification is made in two steps using the "expert system" in both steps: (1) Explicit criteria for classification of each pixel and simple calculations afterward are applied to each ASC image to obtain a simple set of numbers, or "ASC auroral index", representing the occupancy of auroral pixels and characteristic intensity of the brightest aurora in the image. (2) Using this ASC auroral index, the level of auroral activity is estimated, aiming Level 6 as clear Local-Arc-Breaking and Level 4 as precursor for it (reserving Levels 1-3 for less active aurora).

The first step is further divided into two stages: (1a) Using simple criteria for R (red), G (green), B (blue), and H (hue) values in the RGB and HLS colour codes, each pixel of a JPEG image is classified into several categories according to its colour as "visible diffuse", "green arc", "strong aurora" (ordinary green colour by atomic oxygen's 557nm emission is either nearly saturated or mixed with red colour at around 670 nm emitted by the molecular nitrogen), "cloud", "artificial light", and "moon". (1b) The percentage of the occupying area (pixel coverage) for each category and the characteristic intensity of "strong aurora" are calculated.

The obtained ASC aurora index is posted in both an ascii format and plots on a real-time[1]. When Level 6 (Local-Arc-Breaking) is detected, automatic alert E-mail is sent out to the registered addresses immediately. The alert system started 5 November, 2021, and the results (both Level 6 detection and Level 4 detection) were compared to the manual (eye-)identification of the auroral activity in the ASC during the rest of the auroral season of Kiruna ASC (i.e., examined all images during total five months until April 2022, and occasionally double checked in the sky). Unless the moon or the cloud blocks the brightened region, nearly one-to-one correspondence between Level 6 and Local-Arc-Breaking judged by eye using original ASC images is achieved within ten minutes uncertainty.

1 Introduction

In spaceweather monitoring and real-time studies of the ionospheric/magnetospheric science, real-time broadcasting the monitoring results by web or other method, i.e., nowcasting the local geomagnetic and ionospheric conditions is as important as

[1]https://www.irf.se/alis/allsky/nowcast/

monitoring the upstream conditions. Here, the upstream condition includes the solar wind and the interplanetary magnetic field (IMF) conditions at the Sun-Earth Lagrange (L1) point, and the detection of the coronal mass ejection (CME) and the solar flare at the Sun. Although the upstream monitor provides predictions of global activities, it is difficult to predict and impossible to know the local geomagnetic and ionospheric activities with the upstream monitor only. This difficulty applies even when the local activity is a part of the predicted global activity such as a substorm, with uncertainty of more than at least 30 min and several degrees in latitude and longitude. This means that the location and timing of a high geomagnetic and ionospheric activity are difficult to predict by more than these uncertainties, particularly for events with high risk of the space weather hazards. For such local forecast, monitoring the local condition (such as the geomagnetic field and all-sky cameras (ASC) images) and comparing it with upstream conditions and regional conditions (area covered by several stations) are essential.

Here, aurora condition is known to reflect the magnetospheric and ionospheric conditions (e.g., Akasofu, 1977), and the hazardous magnetospheric/ionospheric conditions almost always cause intense and enlarged aurora. This is why many high-latitude observatories started nowcasting the local auroral conditions (e.g., webcasting the real-time data) after relevant technology becomes ready. Even data from regional network of observations such as geomagnetic array (Friis-Christensen et al., 1988; Luhr et al., 1998) and ASC array (Syrjäsuo et al., 1998; Partamies et al., 2003) are being nowcasted, updating every minute or even more frequent.

Among many traditional methods to monitor the local aurora condition, cost and handiness of ASC decreased drastically during past three decades, becoming the most convenient method to monitor the ionospheric condition, although its operation is limited to night. Fig. 1 shows an example of auroral image taken by Kiruna ASC[2]. In addition to the ASC images, some observatories nowcast the keograms of these ASC images using the north-south slices of the images (see Fig. 2 for the explanation of the Keogram). These data are normally archived in the Joint Photographic Expert Group (JPEG) format, and these JPEG files are actually used for auroral, ionospheric, and magnetospheric researches, including event searching.

Handiness of the ASC data also stimulated non-specialists of the aurora to use the ASC data. These potential users include electric power companies, satellite community (scientists, engineers, and operators) except those engaged with optical instruments, and even tourists and aurora enthusiast. However, these potential users are normally not familiar to interpreting the ASC auroral images nor keograms. For examples, different aurora forms (ratio of different types of aurora) means different magnetosphere-ionosphere current systems for different conditions, such as different UT and different phase of the aurora cycle (about 1-2 hours). Understanding these differences used to require both background knowledge of relation between various aurora and various magnetospheric and ionosphere activities in addition to actually watching the aurora in the naked eye (Akasofu, 1977). Thus, judging the auroral condition requires more than judging the simple morphological difference (existing machine-learning method has not overcome this problem as mentioned below). Considering wide possible users, the activity level of the aurora based on the expert judging, in addition to the keograms, should also be nowcasted as guidance.

One way is producing an index that is composed of a simple set of numbers. The idea is similar to real-time AE nowcast by the world data center (WDC) in Kyoto[3] for auroral region and real-time Kp nowcast by Helmholtz - German Research Centre

[2]archive is found at https://www.irf.se/alis/allsky/krn/yyyy/

[3]https://wdc.kugi.kyoto-u.ac.jp/ae_realtime/presentmonth/index.html

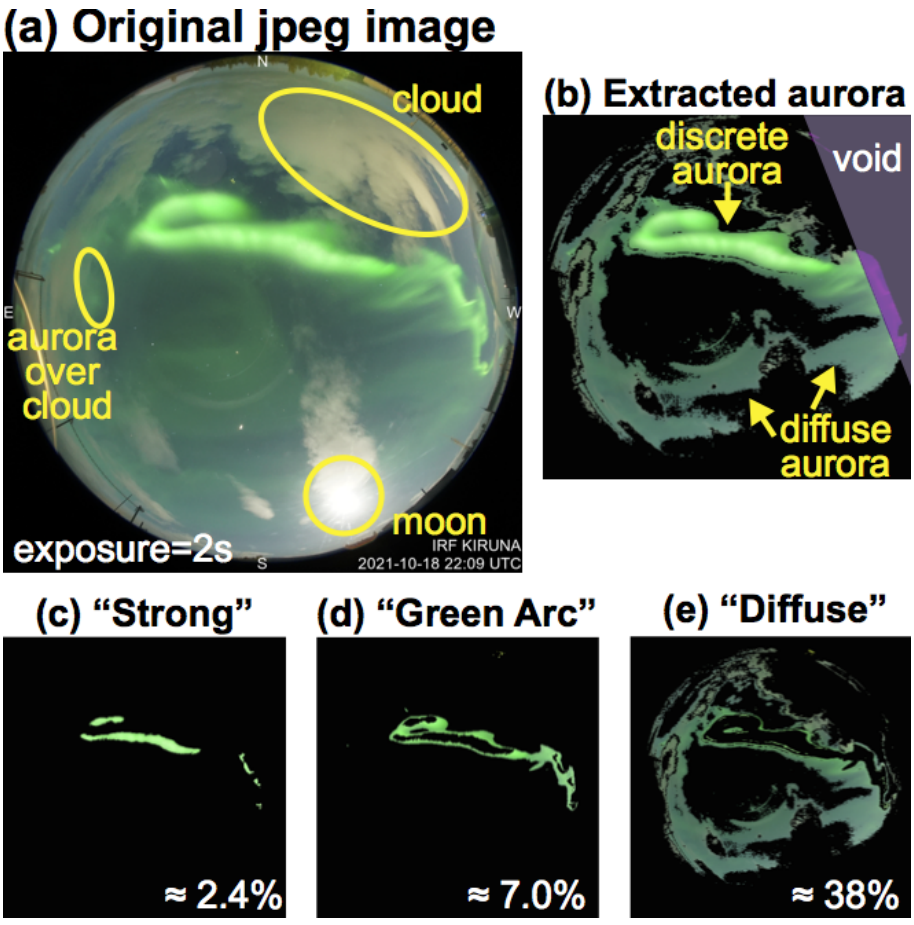

Figure 1. The all-sky image and processed images of 18 October 2021, 22:09 UT, taken by Kiruna all-sky camera (ASC). The automatic exposure time for this particular image is 2 sec (second shortest due to the moon). Auroral emission is characterized by green colour at 558 nm wavelength. (a) ASC image before the analyses (low-resolution JPEG with 482×482 pixels) that is shrunk from original image (2832×2832 pixels). Basic categories of aurora (discrete and diffuse), cloud, and the moon are marked in the figure. (b)-(e) Processed images by the automatic identification of each pixel (present method), extracting (b) all aurora pixels (window is 430×430 pixels), (c) only "strong aurora" in the present definition, (d) only "green arc", and (e) only "visible diffuse". In the analyses, we mask all pixels more than 215 pixels from the center and also upper right corner (purple-shaded region in (b)) because this part is normally contaminate by the city light (located in the west of ASC).

for Geoscience (GFZ) in Potsdam[4] for sub-auroral region. Another analogy is the moment data (density, velocity, pressure) calculated from particle spectrometer. Such an "index" allows even scientists on aurora to overview the activity during the recent one hour through line plots of the index values.

[4]https://isdc.gfz-potsdam.de/kp-index/

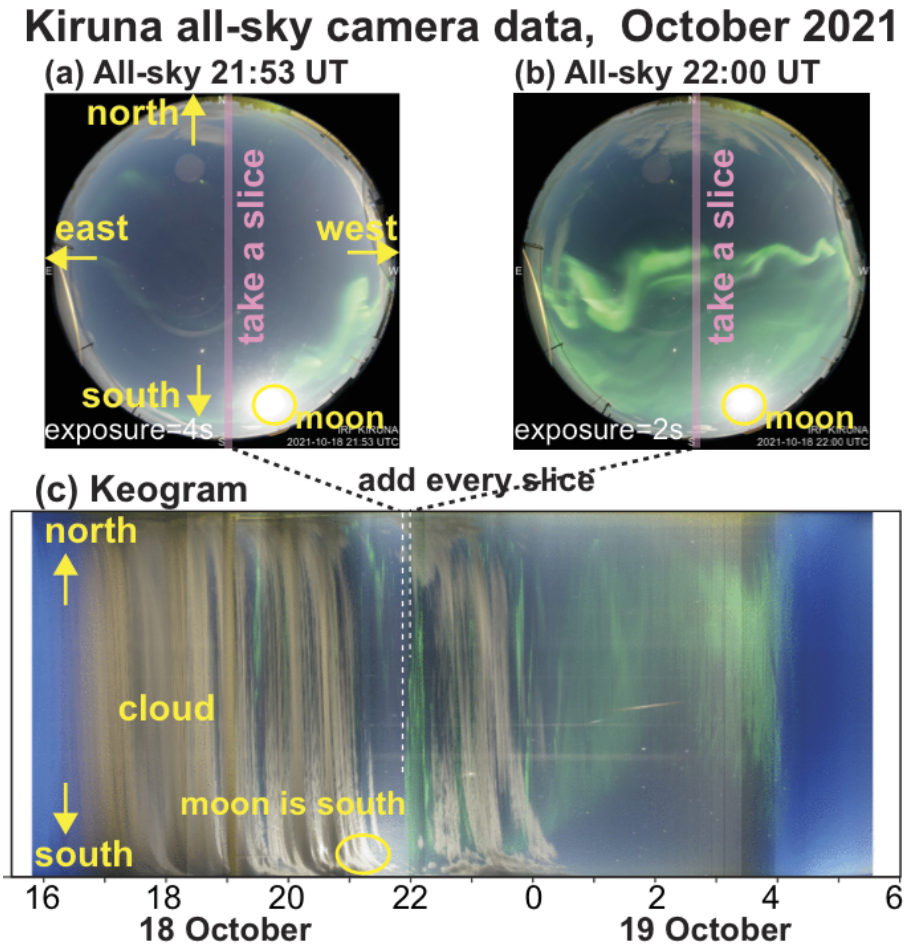

Figure 2. An example of the keogram that is created from a time series of the all-sky camera (ASC) images. Upper panel shows the ASC images during the "Local Arc Breaking" (see text for explanation): (a) 21:53 UT with 4s exposure, and (b) 22:00 UT with 2s exposure. Only the north-south slice of each image (red-hatched area in the middle) is used to create (c) keogram, a time series of the activity (but mixed exposure time as it is) seen in the north-south meridian.

In both the geomagnetic indices and moment values, these simplified "numbers" are used to judge the level of geomagnetic and plasma activities, respectively. Likewise, the set of numbers calculated from the ASC images can be used to evaluate the auroral activity level, such as the sudden and significant intensification of auroral arc with expanding motion (we call it "Local-Arc-Breaking" hereafter). This "second step" classification (judging the activity level from a set of numbers) opens up a possibility of the real-time alert of high activities including the Local-Arc-Breaking. The sequence of aurora shown in Figs. 2a, 2b, and Fig 1a (21:53 UT, 22:00 UT, and 22:09 UT, respectively, on 18 October 2021) is an example of the Local-Arc-Breaking, as characterized by northward quick and expanding motion of the brightest green aurora. The motion is also recognized in the keogram (Figs. 2c).

The concept of this aurora classification in terms of the activity level is similar to the "class" that is used for cyclone/hurricane. The simple formats using indices or levels have another merit in observations: it becomes easier to switch to burst-mode monitoring and to make the post-event analyses such as event identification and statistics. For example, ASC images can be taken more frequent (like with 5-10 sec resolution) than with nominal 1 min resolution during high level period, allowing us to keep the archiving size as small as possible.

The question is then (1) how to define and calculate these numbers from the auroral image and also (2) how to derive the activity levels from these numbers. Thus, the task can be divided into two parts, with the first part evaluating the contributions from different light sources (e.g., aurora, moon, cloud), and make it as simple as possible but with sufficient information to evaluate the activity level. A successful result of (1) should make part (2) easy.

For the first part (1), a combination of simple criteria is applied to each pixel to classify into the different light sources, after which simple calculations are made to obtain the index for an entire image (a simple set of numbers including occupancy percentage). This part requires real-time processing of about 150000 active pixels (each pixel has a 6 byte colour information). For the second part (2), we define the activity level using only the index values, by applying simple set of criteria, without using any pixel-level information. In other words, we aim step (1) producing a set of numbers sufficient for judging the auroral activity level. By doing so, time series (e.g., past 20 min values) of the set of numbers may even be used for short-term prediction, for example, over next 5 minutes, in the future.

We use the expert system for both parts (1) and (2). One (minor) reason using the expert system is that the computation must be performed within small resource, equivalent to a personal computer that is normally used on many ASC sites. For the first part (classifying each pixel), it would be ideal to use the neighbouring pixels together, but that requires too much computation resource for low-performance processors. Therefore, we classify each pixel independently in the present version (ver. 1) except for judging the moon that occupies a solid small area (radius at least 5 pixels and often about 10 pixels) with nearly white colour.

The main reason for using this two-step expert system is, on the other hand, to translate the traditional manual method to the numerical algorithm as much as possible in both evaluating the auroral activity and judging the Local-Arc-Breaking by watching the sky (e.g., Akasofu, 1977). Such manual judge used to be done first evaluating the colour information to judge any emission is aurora or not, and then evaluating the activity level from both intensity and area. Fortunately, the pixel-level identification of the aurora emission is possible because the most outstanding auroral emission for human eye is 558 nm (green) line emission from the atomic oxygen, and this wavelength is quite different from other non-auroral emission in the night sky. Note that just using green colour intensity in the Red-Green-Blue (RGB) colour system cannot distinguish cloud and the moon from aurora because the white light include green colour component. Nevertheless, the colour corresponding to the green aurora is quite different from the other light source in the RGB colour space.

The present method is the first trial of such full translation to the full operational level (in fact, it is in operation over one season). Surprisingly, there has been no automated scheme of quantifying the activity level of aurora, particularly the Local-Arc-Breaking (at least the authors are not aware of) that is the most important event in the ionospheric and magnetospheric activity. Several groups have started identification (even classification) of aurora using machine-learning methods (eventually

deep learning neural network) directly from ASC images (e.g., Clausen and Nickisch, 2018, Kvanmmen et al., 2020; Nanjo et al., 2021, and references therein). The machine-learning is a powerful and rapidly developing tool and even the real time classification is implemented using deep learning neural network (Nanjo et al., 2022)[5]. However, what so far exists is only classifying the entire sky into different categories, starting from "training set".

For example, Nanjo et al. (2022, Fig. 1) and its reference (Clausen and Nickisch, 2018, Fig. 1) have three auroral categories "arc" "discrete" "diffuse" as one value for each picture (here "arc" is just only a special form of "discrete" from auroral science viewpoint), but "discrete aurora" and "diffuse aurora" always appears together for all active aurora or during the precursor of active aurora. Also, no machine-learning method has quantified the intensification of the discrete (arc) aurora (at least the authors are not aware of) although such quantification in inevitable in judging the Local-Arc-Breaking. Since most of the auroral images are mixed with cloud (it is very rare to have clear sky during night), the classification of the entire image as one category may often end up "ambiguous" (Clausen and Nickisch, 2018) or "Aurora and cloud" (Nanjo et al., 2022).

Also, a machine-learning method includes a black box that depends strongly on the learning set, and it might be difficult to identify the reason for any error in the judgement. Contrary, the present approach of using the two-step expert system (sets of solid criteria) can easily identify the reason (by auroral scientists) for any error in the judgement, which is inevitable in improving the algorithm for the future version 2, version 3, etc. Furthermore, since the logic and aim for each step is clear in the present method, the method can gain help from the machine-learning method at each step. For example, step 1 may be improved by using the random forest method (Breiman, 2001; Liu et al., 2017). Also, by comparing with the outputs of the expert system, improvement of the machine-learning scheme may become easier.

As the source ASC data, we use JPEG images because this is the direct output from Kiruna ASC (Fig. 3, see below for detail). Since the raw output is too large in size to store massive images (disk space is common problem in all optical observatories), output format of almost all monitoring ASCs are compressed format, and the majority of the compressed format used by ASC camera are JPEG format. Fortunately, the difference in the colour values of each pixel between different JPEG formats (reduced resolution JPEG compared to raw JPEG output from the camera) is much smaller than difference in the colour values between different cameras. The difference is even smaller than the colour difference during different light conditions (moon, twilight, cloud) according to our experience. This is partly because the JPEG compression is surprisingly good in preserving the auroral green colour that is outstanding in the RGB colour space from the other light sources in the night sky.

Therefore, a successful algorithm for Kiruna ASC may open up a possibility of application (with proper modification) to a wide range of auroral cameras, including those owned by schools and private sectors (e.g., Toyomasu et al., 2008). With such wide range of possible application, a successful translation of traditional manual judgement of auroral activity into a numerical scheme (both the classification of auroral pixels and the judgement of auroral activity) would benefit not only science (event identification and clarification of physics behind the classification and judgement) and operations (archiving, satellite, space weather counterpart), but also education and tourism.

[5]https://tromsoe-ai.cei.uec.ac.jp/

Figure 3. All-sky camera (ASC) at Swedish Institute of Space Physics in Kiruna (68° north).

2 Algorithm and source data

As mentioned above, there are two major tasks: (1) to obtain the set of numbers representing the activity (we call "ASC auroral index" hereafter) from the colour information of all pixels (about 1.5×10^5 pixels with a 6 byte colour information each), and (2) to evaluate the activity level from this index. The first task is further subdivided into two steps: (1a) assessment of each pixel using simple mathematical criteria, and (1b) integration of the classification results of all pixels into a simple set of number.

In step (1a), we classify each pixel into different categories such as the aurora (three different sub-categories), cloud, moon, artificial light, and unclassified. The classification scheme is detailed in sections 2.1 - 2.3. In step (1b), these classification and actual values of the colour code are used to obtain some sort of integrated value, such as numbers of pixels and average luminosity of the most intense auroral pixels, as described in section 2.4. Once the ASC auroral index (set of numbers) is obtained, we evaluate the auroral activity level using only these index values. This is described in section 2.5.

The source data images from Kiruna ASC operated by Kiruna Atmospheric and Geophysical Observatory (KAGO) at Swedish Institute of Space Physics (IRF). The ASC is located in a 30 cm heated dome at the roof of the optical laboratory, as shown in Fig. 3, in Kiruna at 68° north. The viewing direction of the ASC image is given in Figure 2a. From September 2020, Kiruna ASC uses Sony α7s (firmware rev 3.2) with a Nikon Nikkor 8 mm 1:2.8 objective fish-eye lens with Iris fully open. ISO is set 4000, and colour temperature (white balance) is set 5000 K during the 2021/2022 winter season. The exposure time is dynamic from 1s to about 30s.

The camera is controlled by a Raspberry Pi 4 computer and set to produce JPEG format (no raw data output due to storage space limitations), with 2832×2832 pixels in size, out of which diameter of about 2700 pixels (about 5.7 million pixels corresponds to the actual sky window). The data is stored on a sufficient size disk-server and made available in real time[6]. In

[6]https://www.irf.se/sv/observatorieverksamhet/firmamentkamera/

addition to the original JPEG files, JPEG files with reduced resolution are also stored in the archive: medium resolution JPEG (924×924 pixels) and low resolution JPEG (482×482 pixels). We use the last type (low-resolution) JPEG output, which has the about the size as JPEG files obtained from the old camera (Nikon D700 camera, in service until April 2020). By using the smallest size of JPEG, we save computation time and can keep continuation from the old camera.

The main objective of Kiruna ASC is to overview the sky with emphasis on monitoring the auroral activity. The camera is configured for night-time observations and it operates with dynamic exposure time in order to be able to observe during twilight conditions. The dynamic exposure makes it difficult to define the ASC auroral index, but it is not the main obstacle for the present method because, like the traditional eye-identification of aurora, we allow classification error in the pixel level judgement of the colour. We only need to classify fairly good (one digit accuracy as mentioned later) for only those (actually aurora more than certain intensity) that are essential in properly defining the activity level. Such tolerance solves the problems related to the JPEG compression, such as the colour difference of between different JPEG compression schemes from the same image, and limited values in the colour with only a 6-bit value (2 bit each for R, G, and B) in each pixel.

2.1 How to classify each pixel

Standard digital cameras take colour images using three CCDs of wide spectrum coverage centered at red, green, and blue colours, respectively. The values of detected intensity by each CCD compose the RGB colour code. Naturally, green aurora (558 nm) is registered mainly as high G, and low R and B values. In version 1.0, we use only this green aurora to judge the aurora pixels. However, any emission other than green aurora makes the colour significantly deviate from 558 nm by increasing red (R) or blue (B) value in the RGB system. Unless the incoming light is filtered at narrow band near 558nm, it is impossible to separate this emission from other light. Even with such filter, the image is contaminated by bright light sources (the moon, artificial light, and cloud reflecting these light) have wide spectrum including green colour, giving high green (G) values. In other words, using only G values in the RGB system is misleading.

Nevertheless, human eye can judge which emissions are from green aurora and which are from other light source in the non-filtered ASC images when the light pollution is not significant (auroral ASCs are normally placed at such sites). The general difference between these objects and aurora is that the auroral pixel has much lower values in R/G and B/G ratio in addition to high G values. We first aim to translate such judgment more exactly to a numerical scheme.

To extract the auroral pixels from pixels with high R values (yet R<G), one solution is to use hue (H) values in hue-saturation-lightness (HSL) colour code, which can be derived from the RGB values. Together with lightness (L) value to set lowest threshold of auroral brightness, we can limit to the colour range (how much it is close to 558 nm) by restricting the range of the H value. Using HSL colour code, we actually made primitive version (version 0) of a real-time classification for old KAGO's ASC (Nikon D700 camera) from November 2016 and April 2020 (see Appendix A for the criteria). Although it could identify many of the Local-Arc-Breaking (Yamauchi et al., presentation at EGU general assembly, 2018), the HSL method does not give high enough accuracy in the identification of the auroral pixels for the SONY camera that is in use from August 2020. To improve the classification accuracy, we use all R, G, and B values to judge each pixel.

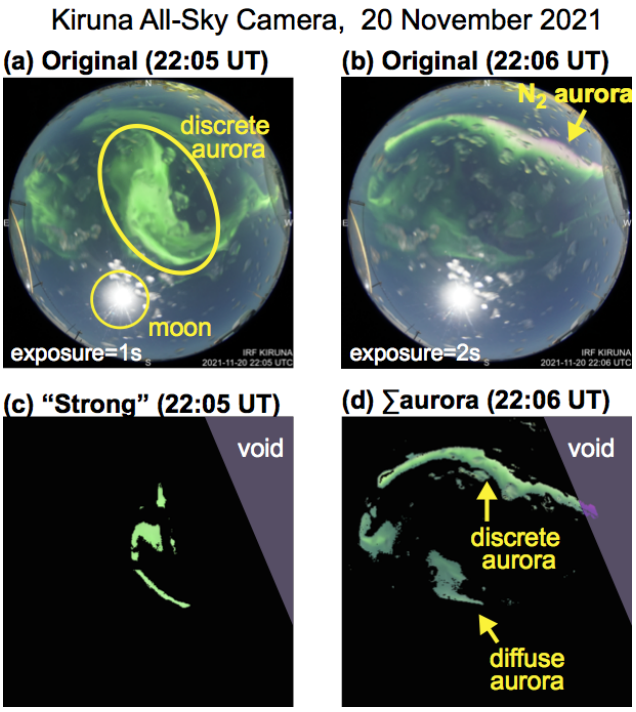

Figure 4. All-sky images of 20 November 2021, at (a) 22:05 UT with 1s exposure, and (b) 22:06 UT with 2s exposure, in the same format as Fig. 1a. (c) and (d) Processed images of (a) and (b) in the same format as 1c and 1b, respectively. The bright spot is the moon, which is removed during the processing.

To classify each pixel using the colour code, we have to identify how large area in the RGB space we can allow a colour as the aurora. Here, we have to consider that the colour significantly deviates from 558 nm even when the non-auroral emissions are ignorable, because the auroral emissions are not only one. Just limiting to main emissions, there are three colours that may mix with the green 558 nm emission: several red emission lines around 670 nm corresponding to the nitrogen molecule (N_2 red lines), few blue emission lines near 428 nm corresponding to the molecular nitrogen ion (N_2^+ blue lines), and different emission line at 630 nm corresponding to the atomic oxygen (O red line). These emissions become strong when the activity is very high, particularly during the Local-Arc-Breaking.

Among them, the N_2 red line (around 670 nm) is often overlapping with the most intense part of the green aurora (558 nm), with only difference in emission altitude (N_2 red line from < 100 km and oxygen green line from > 100 km), resulting the aurora colour shifting toward red. An example of the all-sky image with outstanding N_2 red line is shown in Fig. 4: strong red emissions are found next to (north side of) the main auroral arc in Fig. 4b. This emission comes from the same pixel as the green emission. In this particular case of very strong aurora (Fig. 4), these red pixels are not counted as the auroral pixel simply because $R \leq G$. In version 1.0, we do not included such strong N_2 red line pixels as the aurora pixels because such an aurora is

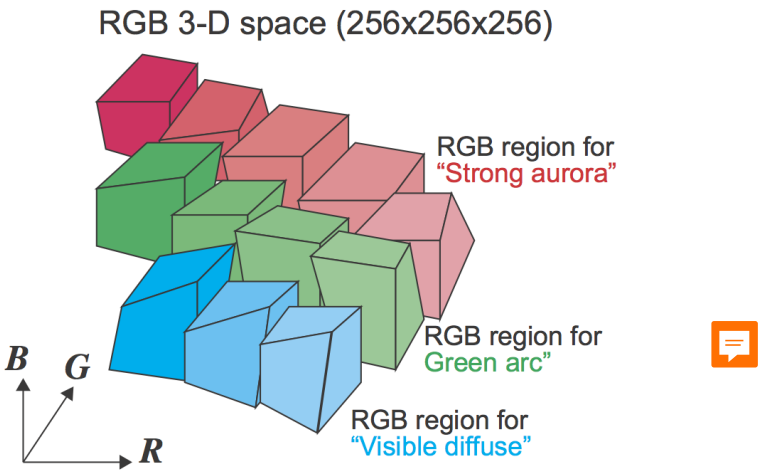

Figure 5. Schematic illustration of how the criteria of auroral pixel are constructed. Each small box with colours represents one criterion ("filter" that we consider safe to judge as aurora. By adding these "safe" criteria (with "or" logic), we can cover wide range of colour (shifted from 558 nm) as the aurora. The actual criteria for auroral pixels are subdivide into three categories (marked as red, green, and blue in the figure). The block shape is not necessary rectangular because we use G, R/G, B/G, and H in different way for different criteria. The exact conditions are given in Table 2. Such a restrictive definition allows a room to add more pixels to identify aurora such as pixels dominated by the N_2 red line (Fig. 4).

normally accompanied by the "strong aurora" on the same image or images ± 1 min as shown in Fig. 4, and does not affect the final judgement of the auroral activity very much.

In most of the cases, the N_2 red line simply increases R/G ratio significantly (shift the colour toward red). Similarly, the N_2^+ blue lines simply increases B/G ratio significantly (shift the colour toward blue). Fortunately, such a pixel normally includes very strong green emission, causing a high G value. Therefore, we can define different threshold for R/G value and B/G value for different G ranges.

The colour shift also comes from the contamination by non-auroral light sources, particularly the moon and twilight, and the level of deviation changes with the exposure time (generally shifting to red for longer exposure time). Therefore, we allow extra colour shift (further deviation from 558 nm) as long as the criteria do not misjudge the non-auroral source as strong aurora in a critical manner for our main purpose. To safely extend the allowed colour range while avoiding misjudgement of non-auroral emissions as aurora, we add small "safe" area one by one, as illustrated in Fig. 5.

Such an exclusive definition has an advantage that we can add new criterion as "or" logic, in case we miss some type of aurora in the present criterion. For example, strong N_2 red line with very little green line (cf. Fig. 4) can be added as a new category after separating its colour code from the twilight.

The final shape of RGB colour area for the auroral pixels are complicated and not smooth, leaving a room of future smoothing the criteria into less numbers of criteria for each category in a similar manner as the principal component method. However, after examining individual pixels, most promising H values for such principal component fluctuates depending on the auroral

luminosity, the moon, twilight, cloud, and artificial light. This problem partly comes from the dynamic exposure (general shift toward red or blue), but the fluctuation exists even for the same exposure time.

The obvious problem with the present method is that neighbouring criteria are not smoothly connected as illustrate in Fig. 5. However, this is not a big problem because, as mentioned above, we accept small errors in the ASC auroral index in obtaining the activity level. For examples, we can accept some uncertainly in judging each pixel in terms of different categories. Some colours may simultaneously belong to different categories (e.g., aurora and cloud) and some colours do not have to belong to any category. Although the default for the latter type of pixels is clear sky without aurora, it can well be dark cloud that does not have enough reflection to be judged as cloud (this happens near the edge of the images).

2.2 Three categories for auroral pixels

For aurora, we define three categories as shown in Fig. 1: most likely "strong aurora" (Fig. 1c), "green arc" (Fig. 1d), and "visible diffuse" (Fig. 1e), respectively. Here, strong aurora means very blight discrete aurora that is mainly seen during substorms (e.g., Akasofu, 1977), in which the G values start saturating (while other values also increases with absolute intensity), or the N_2 red line (around 670 nm, see Fig. 4 and relevant text) is mixed. With relatively large increase of R and B values from the green arc compared to the increase of G value, the colour of the strong aurora becomes closer to white, although we can still limit the definition as the green colour dominant (G is larger than R and B), which is equivalent to $0.167 \leq H < 0.5$ (in practice we limit to $0.19 < H < 0.48$). We also apply the same limitation (the green colour dominance) to the other two auroral categories. In other words, pixels that are dominated by the N_2 red line with R>G like Fig. 4, are excluded in the present version as mentioned above. The green arc category is also meant for the discrete aurora with less intensity, allowing strong diffuse aurora to be misjudged into this category because we do not like to miss the discrete aurora from first two categories. The visible diffuse category is meant for only visible ones while camera can detect a dominant portion of the diffuse that the naked eye cannot normally recognize. In Fig. 1, the discrete part of Fig. 1a is recognized in Figs. 1c and 1d, while diffuse part of Fig. 1a is recognized in Fig. 1e.

Having three categories instead of two (discrete and diffuse) has an advantage because the actual classification is fuzzy and often difficult to judge between discrete and diffuse. By having three categories, we can define "strong aurora" as clearly discrete one. We also dismissed weak diffuse aurora as "dark" because that is not very important to diagnose the activity level. Otherwise, the definition is exclusive, i.e., auroral pixels that do not meet these criteria are not included as aurora. We allow such false-positive cases because such a pixel is normally aurora through the cloud or under effect of artificial light and difficult to observe or to use scientific investigation.

The exact criteria of the auroral pixels (strong aurora, green arc, visible diffuse) are obtained by manual tuning of the condition. Here, R, G, and B values are obtained for each pixel that we manually classified as one of the auroral categories (e.g., "strong aurora"). Table 1 shows an example list of RGB values of pixels for different categories that are manually judgement (by eye) for Fig. 1a. By examining several different pixels for the same category, we can make a list of R, G, and B values for one category for one image. This is repeated for different categories (including even Moon, cloud, etc.), different time, different phase of a Local-Arc-Breaking (before, during, and after), different Local-Arc-Breakings, other types of auroral

Table 1. Example of manual classification and colour values of pixels from an ASC image (18 October 2022 at 22:09 UT, exposure time=2s, Fig 1a)

type	R	G	B	G (%)	H (%)	filter*
strong	171	255	170	100	33.1	N1_995
strong	149	255	155	100	34.2	S1_g95
strong	111	249	128	97.6	35.3	S1_g95
strong	131	242	139	94.9	34.4	S2_g88
strong	112	231	127	90.6	35.6	S2_g88
arc	95	255	123	100	36.1	A2_H36
arc	61	242	103	94.9	37.2	A2_H36
arc	104	221	130	86.7	36.9	A2_H36
arc	82	188	114	73.7	38.3	A2_H36
diffuse	54	172	98	67.5	39.4	W2_H36
diffuse	47	158	90	62	39.7	W2_H36
diffuse	50	155	96	60.8	40.6	W5_h40
diffuse	65	109	96	42.7	45	W5_h40
cloud	167	167	129	65.5	16.7	C3_g60
cloud	169	178	157	69.8	23.9	C4_g64
cloud	179	180	138	70.6	16.9	C3_g60
cloud	218	206	168	80.8	12.8	C3_g60
moon	255	255	255	100	0	M_254
moon	244	244	242	95.7	16.7	M_core
moon	226	224	209	87.8	14.7	M_blight
moon	237	235	220	92.2	14.7	M_blight
moon	197	203	201	79.6	44.4	M_full

* corresponding criterion in Tables 2-4.

activities, and different days with different conditions (e.g., Moon, cloud, twilight). Once the values are obtained, we also calculate the H, L, R/G, B/G, and(R+B)/G values.

After completing the list for all samples, we arrange the list in terms of G and H values for each category, such that we can tune the condition for other values for given range of the G value (and H value). We prioritize the G and H values because these two values are determining factors "how much green" and "how strong is green". Problem is that the allowed ranges of R and B values change for the same category if we change the G values. To exclude the colours that belong to the other category for the same G values, we need condition for colour balance (H, R/G, and B/G) as restrictive as possible. Therefore, we have many "OR" conditions for each category.

Table 2. Criteria of a pixel for strong aurora, green arc, and visible diffuse ("strong", "arc", "diffuse" in the first column, respectively)

category	filter name*1	G	H	R/G	B/G	(R+B)/G	R+G+B
strong*2 (with N_2)	N1_995	0.995≤	0.25≤, <0.34	0.50≤, <0.95		<1.90	
strong*2 (with N_2)	N2_97	0.97≤	0.25≤, <0.34	0.50≤, <0.92		<1.90	
strong	S1_g95	0.95≤	0.26≤, <0.36	<0.75		<1.90	
strong	S2_g88	0.88≤	0.30≤, <0.36	<0.70	<0.66		
strong	S3_g83	0.83≤	0.30≤, <0.34	<0.62	<0.57		
strong	S4_g76	0.76≤	0.32≤, <0.36	<0.43	<0.50	<0.89	
strong	S5_g77	0.77≤, <0.83	0.30≤, <0.352	<0.60	<0.64	≤0.96	
strong	S6_g75	0.75≤, <0.95	0.26≤, <0.31	<0.69	<0.54		
arc	A1_H32	0.69≤	0.32≤, <0.36	<0.47	<0.51		
arc	A2_H36	0.69≤	0.36≤, <0.41	<0.70	<0.80		
arc	A3a_H28	0.65≤, <0.80	0.28≤, <0.35	<0.70		<1.21	
arc	A3b_H28	0.65≤, <0.80	0.28≤, <0.35	<0.70	<0.62		
arc	A4_H24	0.59≤, <0.70	0.24≤, <0.27	<0.80	<0.55		
arc	A5_H20	0.59≤, <0.77	0.20≤, <0.24	<0.92	<0.65		
arc	A6_g55	0.55≤, <0.68	0.30≤, <0.36	<0.61	<0.61		
arc	A7_g50	0.50≤, <0.69	0.25≤, <0.35	<0.75	<0.51		
diffuse (+ light)*3	w0_g85	0.85≤, <0.94	0.31≤, <0.38	<0.92	<0.93	<1.83	
diffuse (+ light)*3	w2_H36	0.61≤, <0.80	0.36≤, <0.43	<0.88	<0.92	<1.70	
diffuse	w1_H30	0.61≤, <0.87	0.30≤, <0.36	<0.83	<0.80	<1.60	
diffuse (arc)≤*4	w3_H24	0.40≤, <0.80	0.24≤, <0.31	<0.72	<0.40		
diffuse	w4_H33	0.40≤, <0.65	0.33≤, <0.38	<0.87	<0.90	<1.70	0.98<
diffuse	w5_H40	0.40≤, <0.65	0.40≤, <0.47	<0.72	<0.96	<1.60	0.98<
diffuse*5 (or arc≤)	w6_H18	0.56≤, <0.75	0.19≤, <0.21	<0.95	<0.6		

*1: The name of a filter (a criterion) that can pick up specific colour range of the aurora pixel, and the final criterion for each category is a summation of different filter under "or" logic.

*2: Contamination from N_2 red line (about 670 nm. see text) increases R/G value.

*3: Contamination by the light is recognized but most likely the visible aurora.

*4: Structured diffuse aurora.

*5: It could be green arc that is reflected by cloud or seen through cloud, but we take safe side not including to the arc.

2.3 Actual pixel-colour criteria for each category

The result for the Kiruna ASC is given in Table 2 for aurora pixels. The criteria are given with AND logic between column, and then OR logic between rows (these OR-logic part is numbered by S1, S2, S3, so on). The exact values of the criterion are camera-dependent, but the deviation of the values for different camera would generally move toward higher or lower values of R, G, B and therefore the modification will not be very difficult for auroral scientists who actually operates the ASC.

Table 3. Criteria of a pixel for the moon and its surrounding (the same format as Table 2)

category	filter name	G	R and G	B and G	
moon	M_254	G_{255} *1 ≤254	R_{255}≤254	-6≤ B_{255}-G_{255} ≤1	
moon	M_core	0.95≤ <0.997	-1≤ R_{255}-G_{255} ≤4	B ≤ G	1.95≤ (R+B)/G <2.01
near moon	M_blight	0.70≤, <0.97	0.994≤ R/G <1.024	0.93≤ B/G <0.98	
affected	M_full	0.60≤, <0.90	0.79≤ R/G <0.98	0.94≤ B/G & B_{255}-G_{255} ≤ -1	0.42≤ H <0.50

*1: R_{255}, G_{255}, H_{255} are JPEG value of R, G, B (0-255 instead of 0-1), respectively

Table 4. Criteria of a pixel for the artificial light ("light" in the first column) and cloud (the same format as Table 2)

category	filter name	G	H	R/G	B/G	other
light	L1_H45	0.65≤, <0.92	0.45≤, <0.67	0.91≤, <1.01	0.92≤, <1.05	
light	L2_H39	0.66≤, <0.74	0.39≤, <0.50	0.88≤, <0.94	0.92≤, <1.00	1.82≤ (R+B)/G
light	L3_H15	0.66≤, <0.74	0.15≤, <0.19	0.94≤, <1.01	0.96≤, <1.00	
light (+ diffuse)*1	L5_g71	0.71≤, <0.92	0.26≤, <0.46	0.91≤, <0.98	0.92≤, <0.99	
cloud + light	C1_g995	0.995≤		0.995≤	0.92≤	B<G-0.018 & B<R-0.018
cloud + light	C2_g94	0.94≤, <0.995	0.10≤, <0.24	0.99≤	0.89≤	B<G-0.018
cloud + light	C3_g60	0.60≤, <0.96	0.10≤, <0.19	0.97≤, <1.10	0.65≤, <0.90	
cloud + moon	C4_g64	0.64≤, <0.77	0.18≤, <0.27	0.92≤, <1.00	0.86≤, <0.96	
cloud	C5_g50	0.50≤, <0.67	0.10≤, <0.20	0.95≤	0.55≤, <0.80	1.52≤(R+B)/G
cloud	C6_g38	0.38≤, <0.55	0.12≤, <0.20	0.92≤	0.50≤, <0.70	1.49≤(R+B)/G
cloud + aurora*2	C7_g41	0.41≤, <0.60	0.17≤, <0.29	0.65≤	0.50≤	B<R-0.10
cloud + diffuse*3	C8_H26	0.60≤, <0.70	0.26≤, <0.32	0.90≤, <0.97	0.88≤	
cloud + diffuse*3	C9_H47	0.55≤, <0.70	0.47≤, <0.55	0.80≤, <0.95	0.95≤	

*1: Similar to note 3 in Table 2, but light effect is stronger than diffuse aurora.

*2: Green arc or strong aurora is above the cloud.

*3: Diffuse aurora is above the cloud.

Criteria for pixels with non-auroral emissions are derived in the same manner as for the auroral pixels. Table 3 shows the results for the "moon" and its surroundings, and Table 4 shows the results for the artificial "light", "cloud" without aurora, and "cloud" but possibly under aurora. As mentioned above, the moon body (characterized by high values of all of R, G, B because of its wide colour spectrum) is obtained from the image as a densely populated solid region of pixels (radius at least 5 pixels) that satisfy the moon criterion. We decided not to use the moon location calculated from the time and the moon orbit because the moon location is displaced by the dome, and the moon is often hidden by the cloud, making the part sky covered by the cloud less affected by the moon (main problem of the moon is its effect on the dome rather than on the sky colour).

In these classifications, some pixels meet two or more different definitions. Therefore, we also give a priority order in the following:

1. the moon (Table 3) and artificial light (Table 4),
2. strong aurora (Table 2),
3. green arc (Table 2),
4. visible diffuse (Table 2),

and 5. cloud (Table 4).

The reason for the first priority is to avoid false negative alert (over estimation of aurora pixel) because false negative is more easily occur than false positive from our empirical experience. Even with very restrictive definition of the auroral pixels, we finally get nearly the same ratio for false negative and false positive in our results. The priority order for 2, 3, and 4 is obvious: among all "possibly auroral pixel", we select aurora pixel, and out of them we select auroral arc (the rest is visible diffuse), and from the aurora arc we select strong aurora (the rest is green arc). The cloud comes as the last priority because this is for estimating the active area, and thin cloud allows strong aurora to penetrate through. In practise, majority of the cloud criterion does not overlap with the aurora definition.

The high priority of moon and artificial light means that some aurora pixels might not be counted, particularly very strong one (such as completely saturated with N_2 red line), if the pixel's colour is judged as the moon or the artificial light. On the other hand, very strong auroral arc without N_2 red line (e.g., G=1.0) is identified as "green arc" or "strong aurora", as long as 0.24<H<0.34.

Some underestimation of auroral pixel due to the saturation is not a problem because what we need is an auroral coverage of approximately 0.05-0.1% accuracy, i.e., about 100 pixels out of 1.5×10^5 pixels (this number comes empirically from the threshold values in evaluating the auroral activity in step 2), and because the major error comes from the fact that a large part of the sky is covered by the cloud and the moon. Because of large number of pixels, we do not need exact a one-to-one relation between the actual type of the aurora and classification category.

Another problem is that the moon modifies the colour toward higher L and higher B/G values at almost all pixels (even aurora pixels far away from the moon) due to the refraction at the dome. This modification is larger at closer pixels to the moon. While better solution for the moon problem (e.g., make the criteria different for different exposure time) will be considered in future, we reduce the moon effect by simply masking all pixels within a certain distance from the moon pixels (14 time of the moon radius that is dynamically obtained) for the present version 1.0. Outside this masked region, the moon effect is moderate, i.e., the diffuse aurora within the masked region will never be classified as strong aurora, and even the green arc is not easily be classified as strong aurora.

Of course, such masking may cause underestimation of numbers of pixels of the strong aurora within this masking distance, although eye identification can judge these strong auroral pixels. Such a coincidence actually happens because the moon is normally located in the south at which the Local-Arc-Breaking sometimes takes place for the Kiruna ASC. Fortunately, after five months of the real-time operation, the number of missed Local-Arc-Breaking due to this coincidence is small (cf. section 2.5) because the aurora often expands beyond the masked region after the Local-Arc-Breaking. In fact, we have enough sample

of Local-Arc-Breaking under moonlight when making a similar table as Table 2. Thus, the present version of dealing with the moon is still effective. Since the moon is characterized by high values of all of R, G, and B, our moon mask would work at other latitude.

We also imposed another mask (void region) in the northwest edge where both the artificial green light source and strong city light is within the field of view, as shaded by purple colour in Fig. 1. Since the light source covers only near the edge of the ASC's field-of-view, we simply remove the entire section from the analyses.

2.4 Calculation of the aurora ASC index

With the classification criteria for each pixel ready (Tables 2-4), we next obtain a simple set of numbers (parameters) representing all pixels. The obvious parameter is the numbers of pixel, or more precisely, percentage of the coverage over the sky out of about 1.5×10^5 active pixels after removing the void region (cf. Fig. 1b). Since we use fish-eye lens (almost all ASC are using some sort of fish-eye lens), there is a strong geometrical distortions, particularly near horizon. Simple correction to this is not perfect solution because distance to the emission region (strongest at 100-150 km) is also strongly distorted near the horizon. Since the distortion is small near the zenith and one can deploy additional camera to compensate near the horizon, we do not include any correction in the present version (v. 1.0). In this sense, this version of the Local-Arc-Breaking alert mainly works for a limited area near zenith. Including the geometrical effect is one of the future tasks (section 4.5).

The strong aurora (which means near saturation or mixture with the N_2 red lines) is normally identified at a small part of the sky even during very active time, and its occupancy in sky ranges normally around 0.1-5% (150 - 8000 pixels, after looking at all plots for the value over 5 months), mainly during and before the Local-Arc-Breaking. For reference, strong aurora pixels in Fig. 1 occupy 2.4% (3387 pixels) of the active area of the ASC. Therefore, an accuracy of 0.03% in numbers of pixels (about 50 pixels) is sufficient to judge the activity level. For the arc aurora that occupies a larger area (normally around 1-20% during and before the Local-Arc-Breaking), 0.1% accuracy in numbers of pixels (about 150 pixels) is sufficient to judge the activity level. Any digit better than these numbers is just a noise in the present case. Therefore, we obtain the coverage of aurora with accuracy of 0.01% for strong aurora and 0.1% for the green arc and visible diffuse. For the other non-auroral categories, our identification accuracy is not better than 1% in the occupied area, but still we obtain 0.1% accuracy when deriving the number.

The simple percentage of the auroral pixels over the sky, however, is not sufficient because it gives higher values for relatively less luminous aurora with wide area than relatively more luminous aurora with small area within the same category. Another problem is that the brightness given as L values is not proportional to the numbers of auroral intensity counted by numbers of photons (Brändström et al., 2012; Sigernes et al., 2014). Therefore, we also define the characteristic brightness of the aurora. Here, we do not take a simple summation of the luminosity values (L in the HSL colour code, that is L=(G+min(R,B))/2 for auroral pixels with G>R,B), because such a summation still gives higher values for wide aurora with low L values than compact aurora with high L values. Instead, we obtain a kind of average intensity of the "strong aurora" pixels, as described below.

If the number of pixels of the strong aurora exceeds 4900 pixels (about 3% of the image), we simply use the pixel data for the most luminous 4900 pixels (judged by the L value) among the "strong aurora" pixels. Here, the threshold number can be actually reduced for the present purpose, but it works anyway (as shown in the result below) and does not affect the computation

Table 5. Content of ASC auroral index

Index content	explanation
%diffuse	occupancy (in %) of visible diffuse pixels
%arc	occupancy (in %) of green arc pixels
%strong	occupancy (in %) of strong aurora pixels (either saturated or N_2 red line is contaminated to the green aurora)
%void	occupancy (in %) of void pixels due to the moon light, artificial light, and obvious cloud that reflects the artificial light
%cloud	occupancy (in %) of specifically the cloud pixels. Note that this is significantly underestimated.
L1	corrected average <L> (luminosity in the HSL) after nonlinear weighting by %arc (and %strong for very small %strong)
L3	corrected average $<L^3>$ after nonlinear weighting by %arc (and %strong for very small %strong)

time. Afterward, we use a nonlinear scheme for averaging. We first take the average of both L values and L^3 values. We reduce the obtained average values if the numbers of auroral pixels are small with the coefficient roughly proportional to $1/\sqrt{n_{arc}}$, where n_{arc} is number of pixel of green arc, and zero when strong aurora pixels are less than 10. Here we use L value as representing the luminosity, but we can use G values because what we are counting is intensity of the green (558 nm) aurora. The exact python code is found in the supplemental material.

Table 5 summarizes the obtained parameters for the ASC auroral index. The index values are stored in an ascii file as the csv (comma separated value) format on a website in real-time every minutes[7]. The real-time plot and the archive of the past data are also found on the same website. For the ascii file, we temporally made its width only 72 columns without tab, which makes the file format very similar to the IAGA2002 format of the geomagnetic field. It is quite possible to extend the column to include other key parameter such as moon position and auroral position, but that will be a future task.

Fig. 6 shows an example of comparison between the index values and the keogram over one night (11-12 March 2022). ASC images when the Level 6 activity is detected was also displayed at the bottom. One can see good correspondence with the index values and keogram image. However, we should note that the present calculations and criteria are made for Kiruna ASC and the classification criteria are different for different camera and different light pollution conditions (e.g., different locations). For example, cloud identification by Sodium line (589 nm) is specific for Kiruna ASC because of strong light-pollution by the city light. This makes identification of cloud relatively simple but identification of weak aurora relatively difficult because the hue (H) values are next to each other. On the other hand, these non-auroral sources do not affect the identification of the strong aurora and green arc because the RGB colour area (particularly R/G ratio for different G range) does not overlap with those for non-auroral light sources. Since we use only strong aurora and green arc categories for the second step (next subsection) in the present version 1.0, the present criteria may well be used for the other location as long as the camera setting is the same. At low latitude stations where the Local-Arc-Breaking occurs in the northward edge, the activity is underestimated due to geometric effect, but the activity in the middle of the sky is still correctly estimated.

[7]https://www.irf.se/alis/allsky/nowcast/

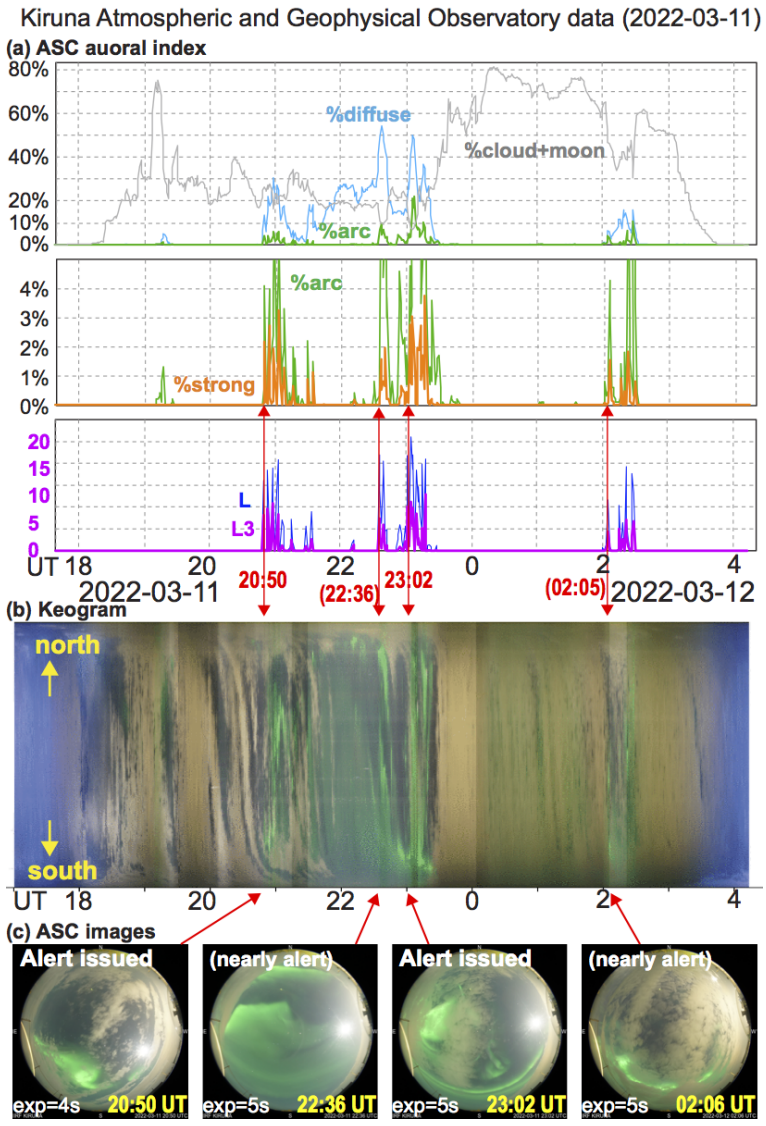

Figure 6. An example of (a) ASC auroral index over one night with both active aurora and occasional cloud 11-12 March 2022. As reference, (b) keogram over the same night and (c) all-sky images at the time of auroral alert are issued for Level 6 activities. Each image is taken toward the sky with north in the top, and hence east (west) is left (right). All images again include the moon or moon-brightened cloud. The automatic exposure time is 4s or 5s for the displayed images.

2.5 Evaluation of the activity level from the aurora ASC index

The next task is to evaluate the activity level from the index values without examining the image data, and then to define the criterion for the activity level that corresponds to the Local-Arc-Breaking (sudden and significant intensification of auroral arc with expanding motion). Here, the "significant intensification" means high values of L1 or L3, with the "expanding motion"

Table 6. Criteria for the activity level (same format as Tables 2-4)

Level	%arc condition	%strong condition	L3 condition
Level 6	$\leq$ 3% (eventually $\leq$2.95%)	$\leq$ 0.2% (eventually $\leq$0.195%)	$\leq$ 8 (eventually $\leq$7.95)
Level 4a	$\leq$ 2% (eventually $\leq$1.95%)	$\leq$ 0.2% (eventually $\leq$0.195%)	$\leq$ 5 (eventually $\leq$4.95)
Level 4b	$\leq$ 1% (eventually $\leq$0.95%)	$\leq$ 0.1% (eventually $\leq$0.095%)	%strong·L3 $\leq$ 1.5%

accompanied by more than certain values of "%arc" and "% strong". Table 6 summarizes the criteria for the activity level (Level 6) that most likely corresponds to the Local-Arc-Breaking in the Kiruna ASC. We also defined Level 4a and Level 4b for auroral activity that is close to but less intense than Level 6, as possible candidates for a precursor of the Local-Arc-Breaking.

Once Level 6 is detected in the real-time ASC image, an alert is sent to the registered mail addresses. We started this alerting system from 5th November 2021. Due to many cloudy nights (particularly during November and December for 2021), Level 6 was detected in limited numbers of nights, but still sufficient to validate this method. In this validation, we examined all ASC images over 5 months by eye (traditional method), and therefore, judgement of the Local-Arc-Breaking is somewhat subjective. Although both authors have watched aurora over Kiruna for more than 30 years while one student independently examined the Level 6 warning, the subjective judging problem always remains. We also examined the magnetometer data because it is another (although much less accurate) indicator for the Local-Arc-Breaking (e.g., Akasofu, 1977; Juusola et al., 2020), but this problem still remains. However, considering its purpose of event identification and real-time warning, both of which also rely on subjective definition, the eye-identification method is sufficient for the validation for the Level 6 definition. Note that this problem also remains with the machine-learning methods because both the sample and results must by validated by eye.

Table 7 summarizes the validation results (Level 6 is detected or not over one night). The table lists the night when Level 6 is detected for each month from 5 November 2021 to 14 April, 2022. Note that from 3 April, the twilight effect makes the detection of Level 6 very difficult and the detection is impossible from 14 April. The night when the present scheme could not detect the Local-Arc-Breaking in the ASC (i.e., false positive) are given as [] except those in very north that are difficult to judge. Unless the aurora brightening takes place very north, above the cloud, or hidden by the moon, the eye-identified auroral brightening is well represented by Level 6 within ten minutes offset.

3 Examples

In this section we show examples of ASC auroral index and ASC images around Local-Arc-Breaking.

3.1 Successful cases

First Level 6 activity after we started the automated mail alert was detected on 6 November 2021, day after we started the system (cloudy on 5 November). Fig. 7a shows the series of Kiruna ASC images around the first Level 6 detection on that day.

Table 7. List of Level 6 alert during 5 November 2021 - 12 April 2022

month	day*1
November 2021	6, 8, 9, 15, [19]*2, 20, [23]*3
December 2021	5, 6, 19, 21, 27, 31
January 2022:	1, 8, 9, 14, 15, 18, [19]*2, 21, 22, 24, 25, 27, 28, 30, 31
February 2022*4	[8]*3, 10, 11, 12, 13,
March 2022	1, 3, 5, 6, [7]*3, 8, 9, 10, 11, [12]*3, 13, [15]*2, 19, 20, 21, 22, 23, 26
April 2022	[3]*5, 7, 12, [14]

*1: Bracket [] indicates that the Local-Arc-Breaking was seen in the image without Level 6 alert.

*2: Moon contamination prevented the identification "strong aurora", with L3=0 for 19 November, L3=6.9 for 19 January, and L3=7.8 for 15 March.

*3: Local-Arc-Breaking in the northern sky only, such that numbers of "strong aurora" did not reach the criterion.

*4: The ASC did not operate on 16-19, and 21 February (total 5 nights).

*5: Relatively weak Local-Arc-Breaking in the dusk sky with some sunlight effect remains, such that exposure time too short to recognize sufficient numbers of auroral pixels.

The ASC auroral index values are given at the bottom of each image. In addition, cloud coverage (in %) is given at the top of each image in Fig. 7a (but not other figures with ASC images). The automatic exposure time (8-10s) is much longer than those of Figs. 1, 2, 4, and 6 (1-5s), partly due to non-moon condition (this is why the city light is outstanding compared to previous images). Each image is taken toward the sky with north in the top, and hence east (west) is left (right).

In Fig. 7a, the Local-Arc-Breaking (most likely the arrival of the auroral substorm bulge to this local time) is seen at 17:31 UT (around 20 MLT) and simultaneously Level 6 is detected, both for the first time in this evening. Before this Local-Arc-Breaking, intensification of the auroral arc equatorward of the original arc was recognised at 17:27 UT (4 min before). In this example, two of three Level 6 conditions, %arc$\geq$3% and %strong$\geq$0.2%, are satisfied from already 17:18 UT, as shown in Fig. 7b, and L3$\geq$8 is the condition that demarcates the activity Level.

As a reference, we also show the geomagnetic variation during this period in Figs. 7c and 7d. Fig. 7c shows fluxgate (DC) magnetometer data and Fig. 7d shows its variation that is represented by three different methods: simple $|\mathrm{d}\mathbf{B}/\mathrm{dt}|$ values using 1s resolution data and 10s-running average (still 1s resolution) data, respectively, and the standard deviation divided by square root of 60s ($\sim$7.75s$^{0.5}$), i.e., normalized fluctuation over 60s. At 17:31 UT when the auroral brightening reached to Level 6, the geomagnetic field suddenly changed, with B_X started changing by more than 100 nT within a minute (this satisfies necessary condition of a substorm) while magnetic deviation increased by an order of magnitude in all three methods.

The next detection of Level 6 activity was under more cloudy condition at 20:43 UT (around 23 MLT) on the same day. Fig. 8 shows the series of Kiruna ASC images, time series plots of the ASC auroral index values and geomagnetic activities in the same format as Fig. 7 except that the cloud coverage is not given on the ASC images. The automatic exposure time (8s and 5s) is the same are slightly shorted than those of Fig. 7. Due to heavy cloud coverage (almost full coverage over the sky), auroral arc before the sudden and significant intensification was not well recognised until one minute before (20:42 UT), at which only one parameter (%arc) reached the criterion of Level 6, while other parameters (%strong and L3) did not reach the criterion of

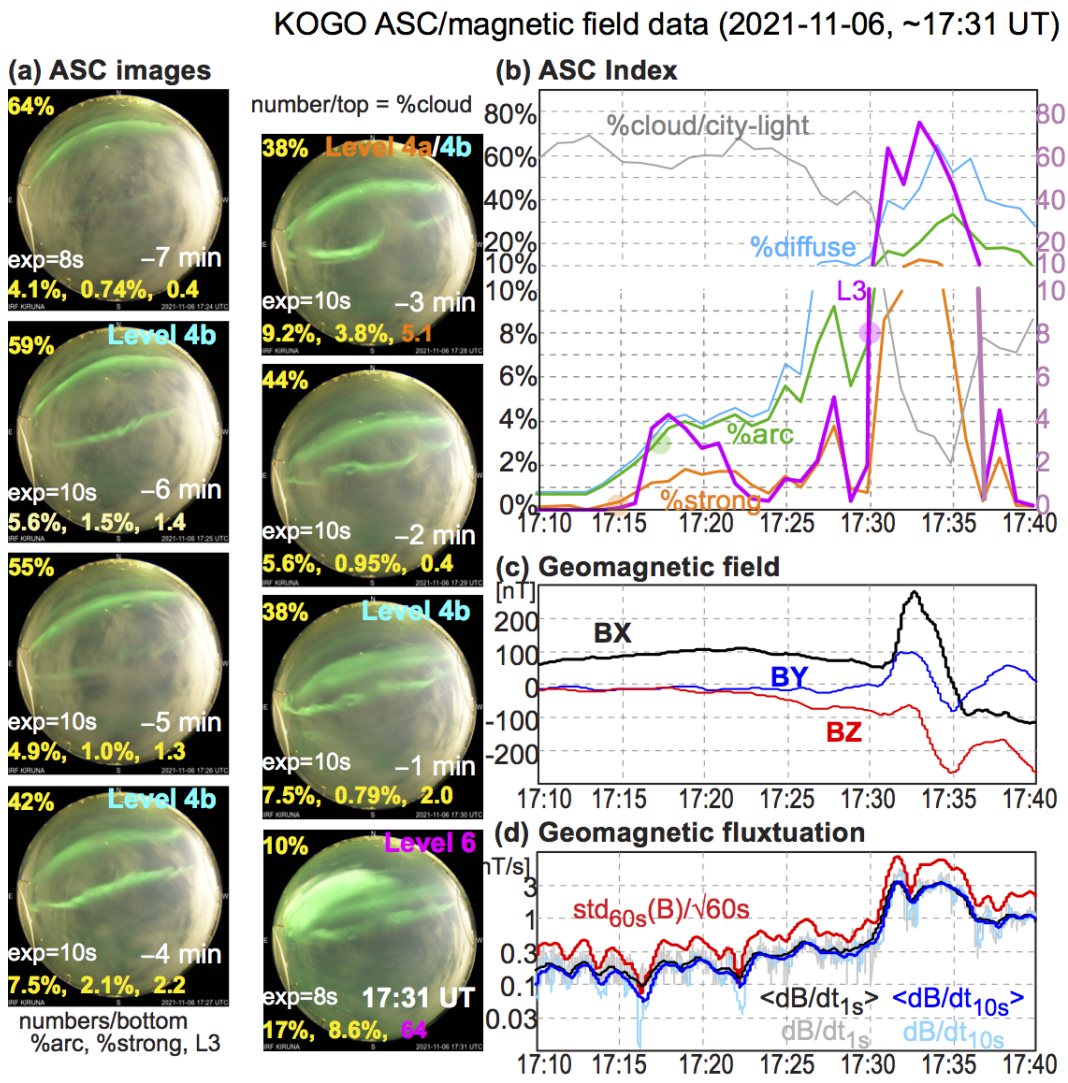

Figure 7. ASC and magnetometer data around 17:31 UT on 6 November 2021, when the fist Level 6 was detected after we started the real-time e-mail alert of the Level 6 activity: (a) Auroral images (the same coordinate as Fig. 2); (b) ASC index values; (c) DC geomagnetic deviation from the baseline values (X=north, Y=east, Z=downward); and (d) AC geomagnetic variation $|\mathrm{d}\mathbf{B}/\mathrm{dt}|$ measured by three different methods. In each image, the ASC index values of %arc, %strong, and L3 are given at the bottom, above which the automatic exposure time and UT are given. The cloud coverage (%cloud) and the activity level (Level 6, Level 4a, and Level 4b) are given at the top. The timing of Level 6 detection is the same as the onset of the Local-Arc-Breaking. In the auroral index panel (b), the scaling is changed between below 10 and above 10 (therefore the graph has a gap in between). The three methods of $|\mathrm{d}\mathbf{B}/\mathrm{dt}|$ are: (1) using 1-sec values (black), (b) using 10 sec running average values (blue), respectively, and (3) standard deviation of magnetic field over 60 sec using 1-sec values and normalised to nT/s unit (red). These variations are first calculated for each vector component, and then taken the absolute values.

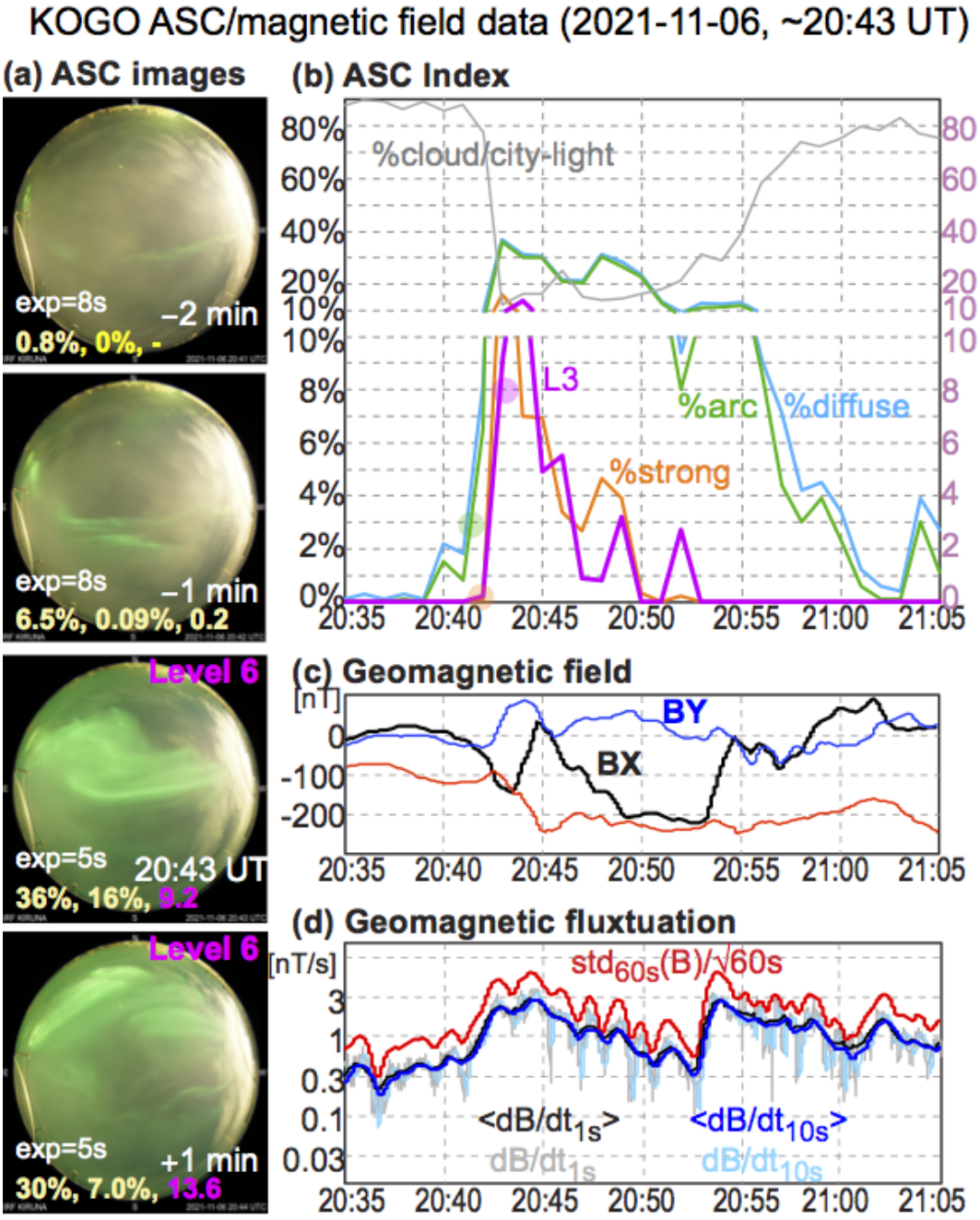

Figure 8. The ASC images, ASC auroral index values and geomagnetic data around the time when the Level 6 aurora activity was detected at 20:43 UT on the same night as Fig. 7. The format is the same as Fig. 7 except that the cloud coverage is not shown on the ASC images.

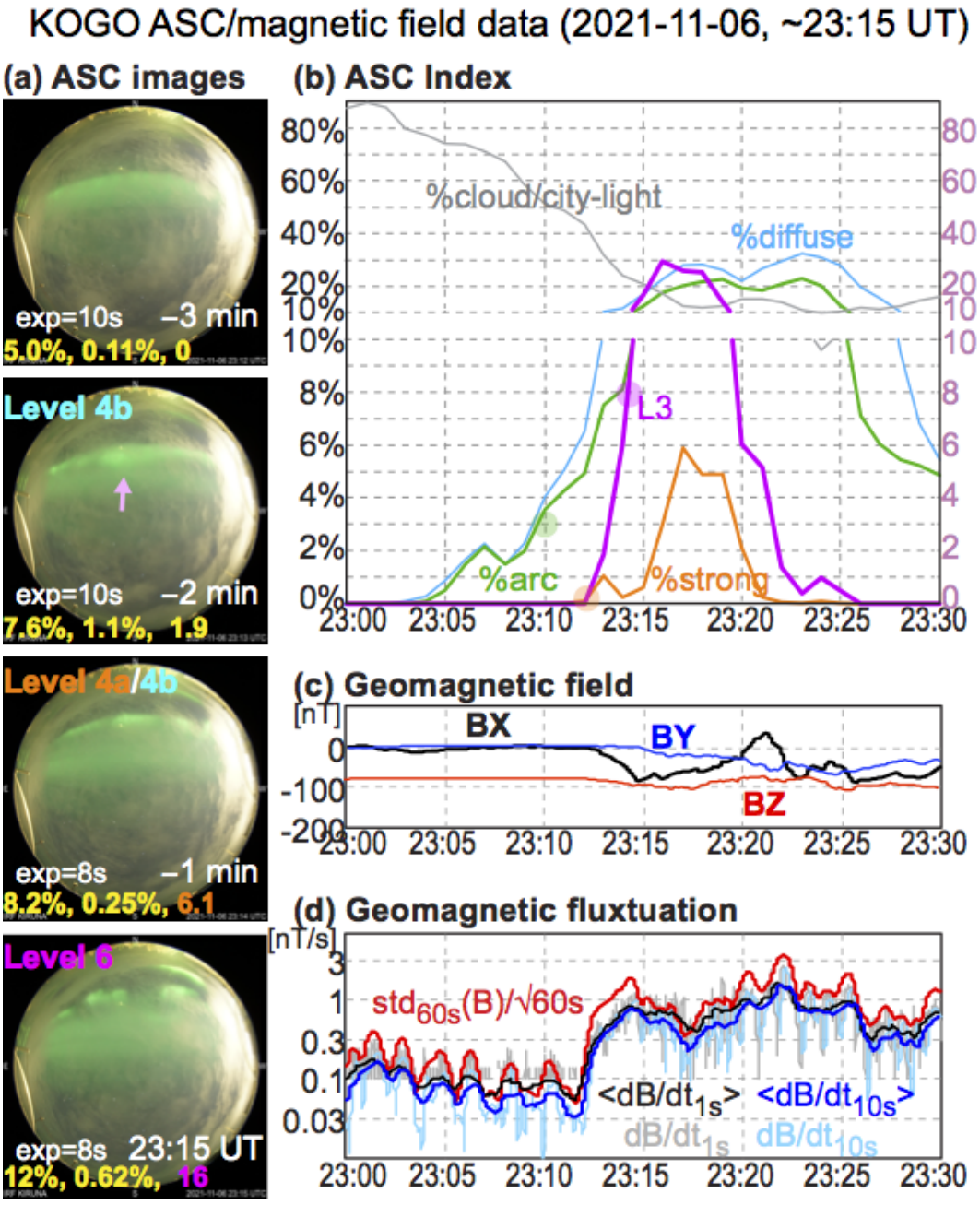

Figure 9. The same as Fig. 8 for the Level 6 auroral activity at 23:15 UT on the same night as Figs. 7 and 8.

Level 4a or 4b. Fortunately the cloud was not very thick and the brightening of aurora was strong enough to be recognized in the ASC auroral index. The timing of Level 6 detection (20:43 UT) again corresponds to a large geomagnetic deviation with more than 100 nT change in B_X and nearly one order of magnitude increase of the magnetic deviation in all three methods.

In both examples (17:31 UT and 20:43 UT), Level 6 detection timing agrees with the timing of the Local-Arc-Breaking in the ASC image, and the morphology the Local-Arc-Breaking is consistent with the evening auroral surge during a substorm (Akasofu, 1964). The last detection of the Level 6 activity on the same night at 23:15 UT took place in the post-midnight sector (around 01 MLT, i.e., post-midnight), where the morphology of the intensification of the aurora arc is quite different from those of pre-midnight (Akasofu, 1964). Fig. 9 shows the relevant images and plots in the same format as Fig. 8. The automatic exposure time (8-10s) is the same as those of Fig. 7. In this example, the aurora brightening started already at 23:13 UT, two minutes before the Level 6 detection, as is also indicated by the geomagnetic deviation (90 nT change of the X component in 2 minutes). Instead of Level 6, ASC auroral index values gave Level 4b at 23:13 UT, and Level 4a at 23:14 UT (%arc=8.2%, %strong=0.25%, and L3=6.1). The magnetic deviation also increased significantly, but the peak values are much lower than previous Level 6 activities (Figs. 7 and 8) by more than a factor of 3. Considering such a small geomagnetic activity and its post-midnight location, two minutes delay of Level 6 detection is still successful for the real-time alert.

Since the intensification of the aurora is quite different between the pre-midnight and post-midnight (e.g., Akasofu, 1964), the relation between the ASC auroral index and the auroral intensification is also different between them. For example, diffuse aurora in the post-midnight is often registered as green arc because of its high intensity. In other words, we need to make different criteria between pre-midnight and post-midnight, and this example may result a different result if we consider the UT information. On the other hand, the present algorithm anyway detects the Level 6 for many of post-midnight cases because the criterion the L3 value is not very much affected. This is why we keep the consideration of the local time as a future task but not very urgent.

3.2 Moon effect

Here, we show two examples with strong influence by the moon: one successful case (15 November 2021, 20:36 UT) in Fig. 10 and one unsuccessful case (19 January 2022, 23:57 UT) in Fig. 11. The examples with the moon in Figs. 1 and 2a also satisfy the Level 6 criterion, and the examples of the Local-Arc-Breaking in Fig. 6 (20:50 UT and 23:02 UT) also satisfy the Level 6 criterion. In Fig. 10, Level 6 was detected at 20:36 UT, which is only 2 minutes after some signature of the Local-Arc-Breaking becomes visible in the ASC. The automatic exposure time (4s) is the same as that in Fig. 2a and similar to those in Fig. 6c, both with the moon. For this event, the brightened aurora is located very close to the moon, and that caused relatively low L3 values and low %strong values. Nevertheless, values of the ASC auroral index reached to Level 6. Comparing to the local magnetometer data (Figs 10c and 10d) that indicate the Local-Arc-Breaking at 20:39 UT, the ASC index gave closer time to the Local-Arc-Breaking.

In the unsuccessful case (Fig. 11), the peak L3 value was only 6.9 at 23:57 UT although the ASC image shows the Local-Arc-Breaking some distance north from the moon. The automatic exposure time is shortened to 2s, the same as those with the moon in Figs. 1a and 2b. Both %arc (=7.0%) and %strong (=0.41%) exceeded the Level 6 criterion at this time, clearing both Level 4a and Level 4b. Thus, only the L3 value did not reach the Level 6 criterion. Both the geomagnetic deviation or > 150 nT within 5 minutes and the magnetic variation reaching nearly 3 nT/s one minute after at 23:58 UT (same level as of Figs. 7, 8, and 10) indicates that aurora activity corresponds to the Local-Arc-Breaking.

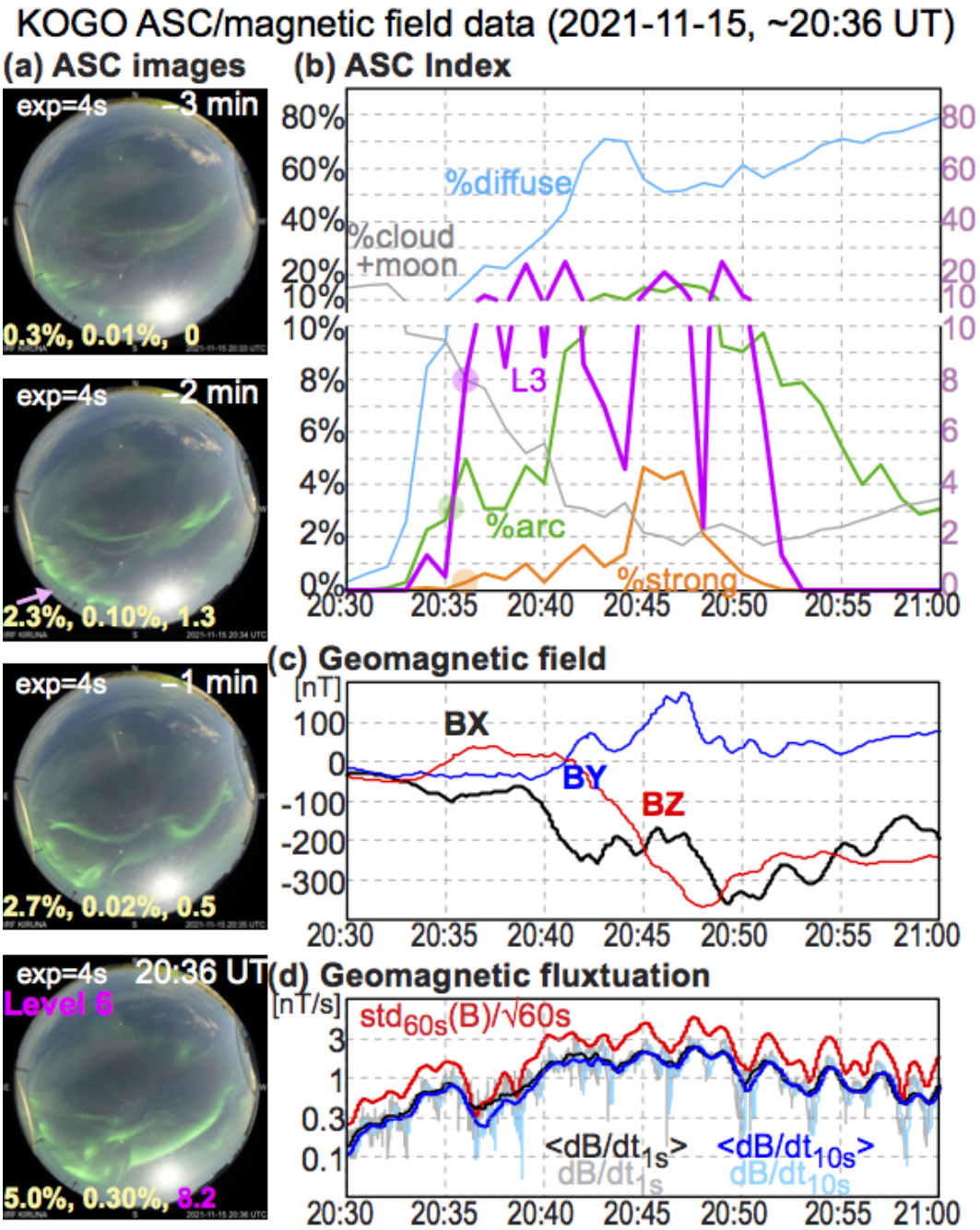

Figure 10. The same as Fig. 8 for the Level 6 auroral activity at 20:36 UT on 15 November 2021.

The small L3 value for this event might partly comes from the change of the colour: background (night sky) colour in the ASC images is more bluish than the ASC images on 6 November 2021. This bluish shift is probably due to the combination of

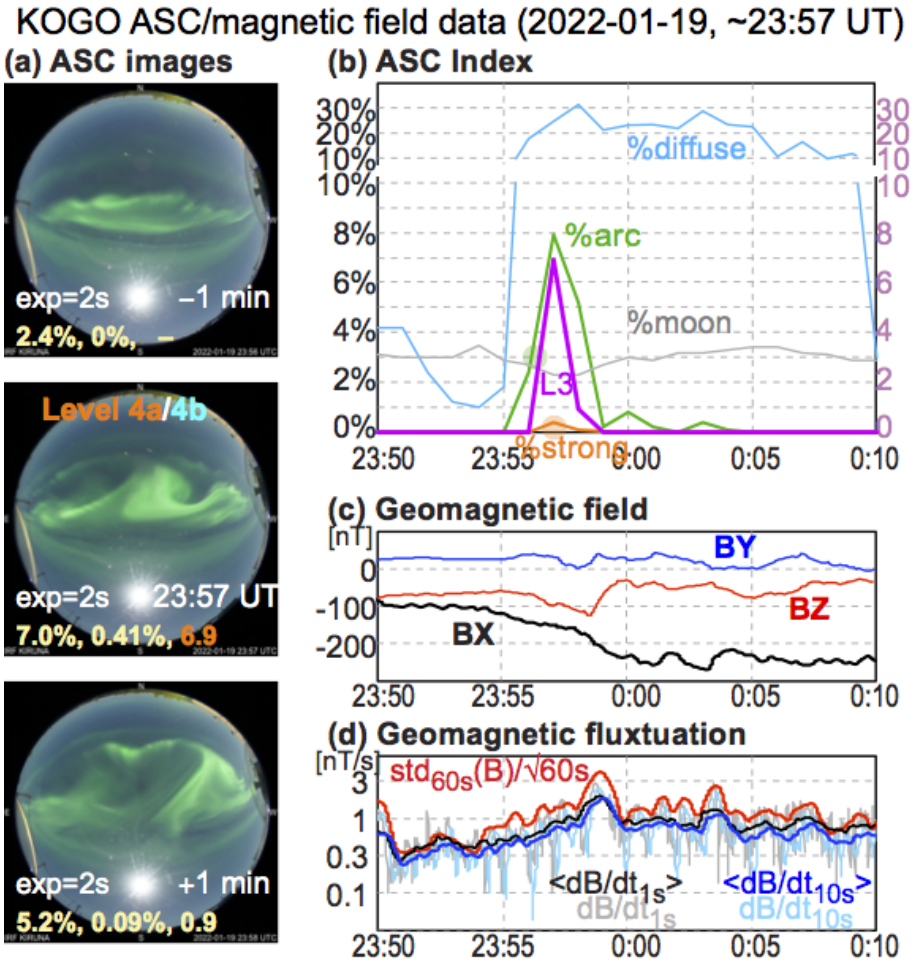

Figure 11. The same as Fig. 8 for the Level 4a/4b auroral activity at 23:57 UT on 19 January 2022.

the wide refraction of moonlight through the dome and reduced exposure time by the existence of the moon. By adding blue colour, the criterion of the strong aurora is affected. Taking care of this problem is one of the future tasks. For the effect of the exposure time, it is not clear how much it affects to the ASC auroral index, according to the examination of the twilight case in Fig. 12.

3.3 Twilight effect in spring and fall

Like the moon effect case, twilight case also changes the colour of the entire image toward blue. Fig. 12 shows one such unsuccessful case. The automatic exposure time (4-5s) is similar to those of the successful moon cases (Figs. 6 and 10). A clear Local-Arc-Breaking took place in the northern sky. In fact the L3 value exceeded the Level 6 criterion at 20:06 UT and 20:07 UT. However, the auroral coverage (either %arc or %strong) did not reach the needed values (marked by blue circle in

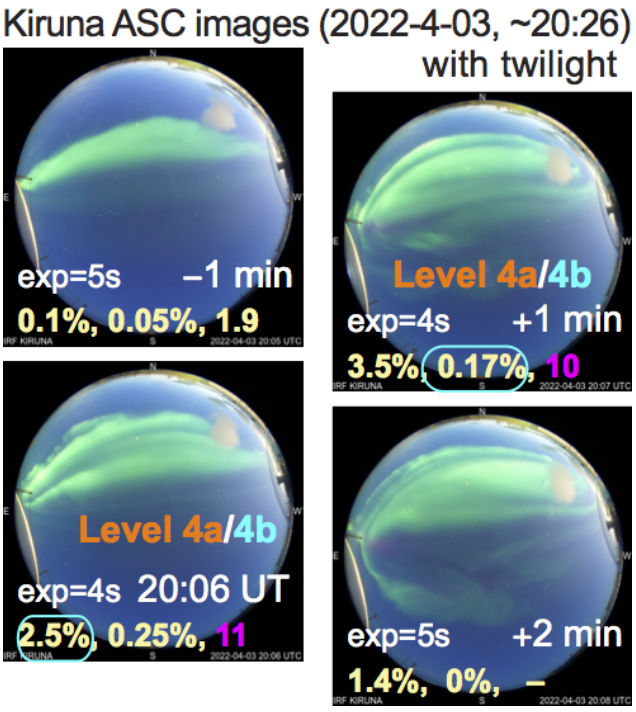

Figure 12. ASC images around 20:06 UT on 3 April 2022, when the ASC auroral index values did not reach Level 6 due to the twilight effect when the Local-Arc-Breaking took place.

the figure). In other words, the short exposure time alone does not prevent the ASC index reaching to Level 6, and therefore we consider the additional blue colour in both the moon case and twilight case might make the auroral pixel more difficult to be identified as "strong aurora".

3.4 Missed case due to northward auroral location

If the Local-Arc-Breaking takes place in the northern sky, the coverage of the aurora (%arc and %strong) becomes small due to oblique looking angle. This sometimes prevents the aurora coverage from satisfying the Level 6 criterion (%arc?3% and %strong?0.2%), particularly for relatively weak Local-Arc-Breaking. Fig. 13 shows one such example of the Local-Arc-Breaking in the far-north part of the field-of-view (23 November 2021, 21:28UT) without reaching Level 6 due to too small auroral coverage. The automatic exposure time (3-4s) is withun the range of successful cases shown In this example, a thin cloud reduced the moon effect, and hence the reduction of the exposure time is not as significant as the unsuccessful moon case (Fig. 11). The most blight image was taken at 21:29 UT with sufficient %strong (=1.15%) and L3 (=9.5) for Level 6, but %arc (=1.9%) was far below the required threshold ($\geq$3%) for Level 6 (marked by blue circle in Fig. 13a). The geomagnetic deviation (Fig. 13c) of more than 100 nT, and geomagnetic variation (Fig. 13d) of about 1-3 nT/s are, considering aurora location far north that causes reduced geomagnetic signatures, large enough to be accompanied by a Local-Arc-Breaking.

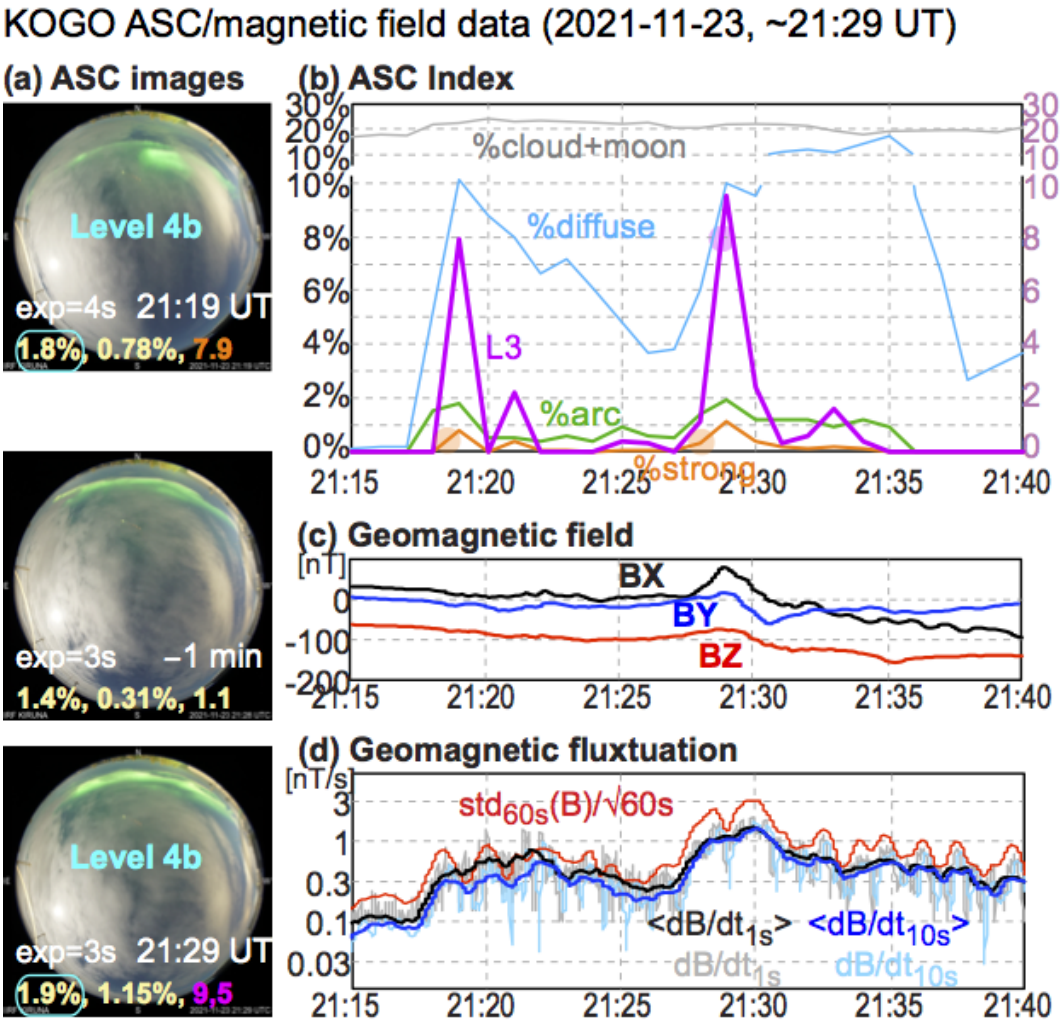

Figure 13. The same as Fig. 8 for the Level 4b auroral activity in the north at 21:29 UT on 23 November 2021.

4 Discussion and future tasks

We used three categories of aurora instead of two (discrete aurora and diffuse aurora). Adding a third category between two different phenomena is a common practical method in classifying data when the criterion is not very much discrete (i.e., somewhat fuzzy) as shown in Fig. 1. Since our aim is to identify the intensification of aurora rather than aurora itself, adding a third fuzzy category between the discrete aurora and diffuse aurora is even more useful. For the same reason, one may add a new category of "could be aurora" that does not reach the criterion of "visible diffuse" if the purpose is just to identify images that may contain visible aurora. The last one is particularly useful for automated removal of ASC image from the archive (with the condition of no aurora and high cloud coverage).

Table 7 lists date that Level 6 was detected. Almost all detection are accompanied by the Local-Arc-Breaking within 10 min, with most of the false negative (detection of Level 6 without Local-Arc-Breaking within 10 min) during intensification of auroral arcs before Local-Arc-Breaking or during the expanded auroral activity like substorm expansion phase (Akasofu, 1977), and are related to the same series of aurora activity related to the Local-Arc-Breaking. Only a small fraction of such intensification was un-associated with substantial expansion of the aurora (about 10%).

Likewise, the present method gave small percentage of false positive: The Level 6 auroral activity was not detected only 9 nights out of nearly 50 nights with the Local-Arc-Breaking in the ASC. After removing the Local-Arc-Breaking that is affected by moon or twilight, this ratio decrease to 4 night out of about 45 night. Even if we count individual Local-Arc-Breaking when multiple events take place in one night, this low false rate does not change very much. Thus, the Level 6 definition in the present version (version 1.0) works as the event identification purpose for both real-time campaign and statistical studies.

In the present expert system, we quantify the auroral activity by using a set of simple criteria and calculations as a numerical translation of how the auroral scientists used to judge the auroral activity (e.g., Akasofu, 1977). Thanks to this quantification ability, this expert system gave a satisfactory result as the aurora alert system after 5 month's operation. The quantification ability is the main difference from existing machine-learning schemes (e.g., Nanjo et al., 2021 and references therein): none of them has yet quantified the auroral activity (neither corresponding to ASC auroral index or the activity level).

Nevertheless, there is considerable room for future improvements. One advantage using simple criteria is that it is relatively easier to pinpoint the reason why the false warning (Level 6) is issued compared to neural networks (or other black-box method). For example, the mid-term product of each category in the first step (derivation of the ASC auroral index) is stored as a masking matrix of $\sim 1.5 \times 10^5$ pixels with true and false values for each category. Therefore, one can examine pixel by pixel in any case of categorizing wrong. This method is actually used to separate the cloud effect during the development of the criteria (Tables 2 and 3). In addition, we have already identified the reason for the false positive for the moon cases: due to the colour shift of all pixels toward blue. All pixels are affected because of the refraction through the all sky dome, and one possible improvement is, in addition to masking, correcting B values by reducing some percentage. The goal is to make the similar values of the ASC auroral index (for strong aurora and green arc, at moment) for the same level of aurora between with and without the moon.

Another advantage of the present method (expert system) is that we do not have to change the entire logic but only to adjust the criteria for different ASCs at different locations that have different light conditions and for different camera manufactures/-models that have different colour characteristics. The auroral morphology is also different at latitudes, but that does not alter the identification of the Local-Arc-Breaking very much. As mentioned in the introduction, adjustment of step 1a can be performed with a help of machine-learning method in the future without changing the other part of the processing. The goal is again to obtain the similar ASC auroral index values for the same level of activity. By doing so, the second step can be processed with the similar criteria as the present one. Likewise, the machine-learning method may help improving step 2 only.

Below are the tasks for future improvement that we consider from the present version (ver. 1.0) in addition to obvious task: tuning the criterion values (e.g., 2.8% instead of 3.0% for %arc in the Level 6 criterion, etc.).

4.1 Correction using exposure time information and UT information (ver. 1.1)

The present version is made to judge only from the JPEG image, but not using hidden information, such that the analyses code (see supplemental material) can be easily modified for the other ASC images, e.g., taken at non-scientific station (Toyomasu et al., 2008). However, we can use two extra information that are available in the most JPEG images. One is the UT information that is tagged to the ASC images in most of the places. The other is the exposure time given as hidden information of the JPEG file (can be extracted with, e.g., "exiftool" command, for python program). So far we have managed in identifying the Local-Arc-Breaking (Level 6) for different UT and for different exposure time, but both the ASC auroral index and activity level definition will be improved by including these information. For example, post-midnight diffuse aurora during a substorm is often too strong and misjudged as the auroral arc (category "green arc") although such an overestimation does not effect the judgement of Level 6 and Level 4b very much. These improvements require further subdivision of auroral image in terms of the UT and exposure time (e.g., two or three different UT ranges and three or four different ranges of the exposure time), which requires much more auroral examples to examine than what we have used so far.

4.2 N_2 red (670 nm) line (ver. 1.2)

In the present version, all auroral pixels must satisfy R<G and B<G (the same as $0.167 \leq H < 0.5$) to avoid any contamination from white light or twilight. This automatically removes the strong red emission by N_2 around 670 nm (mainly < 100 km altitudes) as shown in Fig. 4b, or faint blue emission by N_2^+ at 428 nm (mainly > 150 km altitude). Adding these lines, particularly the strong N_2 red line, would improve the "strong aurora" definition. Fortunately, the N_2 red line in Fig. 4b does not belong to any category yet, opening up a possibility to add a new category "N_2 aurora". To add this category, we must examine more examples with strong N_2 red lines (they are rare) to find out the relevant RGB colour code while limiting to the RGB colour range different from the twilight, moon, and other light sources. Among these non-auroral red colour sources, twilight can be removed from the UT information and location of the red-colour pixels. Priority is lower for extracting the N_2^+ blue line than the N_2 red line because the N_2^+ blue line appears more often near the equinoxes than winter, and including the N_2^+ blue line may cause inequality between different seasons.

4.3 Moon filter and twilight filter (ver. 1.3)

To reduce the moon effect, we currently mask all pixels within a radius that is 14 times the detected moon radius (even the radius of the moon changes with time, location, and moon phase) because both the sky and the all-sky dome scatters the moonlight, modifying the colour and intensity of the auroral pixels in a wide area around the moon during almost all moon phases. Of course the moon itself blocks the aurora at its vicinity.

Just masking the moon from date and time is not easy because the all-sky dome modifies the moon location and size. Also, the effect (shift of the colour toward blue) is seen at almost all pixels of the entire image, with higher effect at closer to the moon. One possible counterpart is to use "corrected B" values that are reduced from the obtained B values, depending on the distance from the moon. The optimum correction needs examination of more samples of aurora with the moon. We can make

the similar correction for the twilight, but this is not as urgent as the moon correction because the twilight problem is seen only at the beginning and end of the season when the night is very short.

4.4 Defining less intense but sudden intensification as Level 5 (ver. 1.4)

Some Local-Arc-Breakings are more compact and less intense than others. Some of them are even difficult to distinguish from simple intensification or deformation of auroral arcs, e.g., expansion of bright region or only nearly breaking that soon returns to the green arc again. Therefore, it would be useful to have a category of minor sudden intensification as Level 5. Such introduction of "fuzziness" makes the alert system more reliable.

4.5 Dividing field-of-view (ver. 2)

The present ASC aurora index treats all pixels equal, which makes the zenith aurora weighted more in the calculation of the index values than the other part of the sky due to the physical geometrical effect while another type of weighting is introduced by the fish-eye lens' optical geometry. Furthermore, the Local-Arc-Breaking in the south sky expands toward the entire sky (Akasofu, 1977), giving higher values than the Local-Arc-Breaking in the northern sky that expands mainly toward northern edge. These "auroral location" problems (reliable only near the zenith or slightly south) should ideally be solved by placing many ASCs within 100 km distance each other. Meanwhile, we can make some improvement with a single ASC by dividing the field-of-view into two-three areas (north, middle, south) and obtaining the index values for each area, in addition to introducing simple correction that depends on the zenith angle. When calculating the final index values, we can weight differently between there three regions (more weight for the northern sky than southern sky). The detailed scheme needs tuning after examining more samples.

4.6 Previous 5-min activities (ver. 2)

For some Local-Arc-Breaking cases without the Level 6 alert, its criterion is satisfied if we take peak values of the ASC auroral index within 5 minutes (4 cases out of 8 nights in Table 7). On 8 Feb, 2022, L3 and %strong are well above the Level 6 criterion at 20:02 UT and 20:03 UT (but %arc = 2.6%, i.e., lower than required 3.0%), whereas %arc and %strong is satisfied at 20:06 UT but L3=6.7. On 7 March 2022, %arc was 3.9% at 18:28 UT, whereas L3 and %strong exceeded the Level 6 criterion at 18:31 UT. On 12 March 2022, L3 and %strong exceeded the Level 6 criterion at 21:45 UT, only one minute after %arc satisfied the criterion (=4.3%). Finally, on 3 April 2022 (Fig. 12), the index values did not exceed Level 6 just because of %arc did not satisfy the criterion (=2.5%) at 20:06 UT and %strong did not satisfy the criterion (=0.17%) at 20:07 UT. Other values during these two images exceeded the Level 6 criterion.

These examples suggest a possibility to loosen the criterion by using nearby data. Other possible solution is to introduce gradients of values such that sharp increases of %strong and L3 as the condition to ease the criterion. Such attempts are also useful in defining Level 5 and lower level of activities. Problem is that the optimization requires complicated examinations of

multi-minutes data, and finding the solution is not simple. This could be a good task to use the machine-learning methods for optimization.

4.7 Precursor or Level 4 (ver. 2)

As the extension of the previous task (considering previous 5-min activity), we can even search precursor signatures of the Local-Arc-Breaking. Level-4a and Level-4b are defined as the first step for this effort, and the methods mentioned above (including machine-learning methods) will help tuning Level 4. In case of using the machine-learning method, only the ASC index values during past 10 minutes should be used to predict Level 6 activity without examining the image data. Then, we can define the ASC auroral index values between 5 min before the Level 6 and 10 min before the Level 6 can be a good candidate of set of values corresponds to Level 4.

4.8 Adding geomagnetic variation (ver. 3)

As an external index, geomagnetic activity can be used to help defining the level. To evaluate the optimum information for this purpose, we showed geomagnetic variations in Figs s. 7-11, and 13 in both DC and AC formats. As the AC variation, we showed $|\mathrm{d}\mathbf{B}/\mathrm{dt}|$ values obtained from the 1s resolution values and from 10s resolution values, and their 1-min running averages, respectively. We also showed theoretical accuracy of the 1s resolution values, i.e., standard deviation divided by square root of 60s, giving the result with the same unit [nT/s] as other parameters.

Change in B_X (deviation within 10 minutes or so) is the optimum parameter for DC variation, whereas all AC profiles are similar to each other, suggesting that using 10-sec values is sufficient as the source data when 1s resolution data is not available. On the other hand, the standard deviation method might be optimum if the computation time is short enough. To find out the optimum one, we need to examine more cases, which needs another solid analyses (e.g., Juusola et al., 2020). This problem is directly related to the geomagnetically induced current (GIC) during the spaceweather hazard events. That is, we can even search for possible precursor of the big GIC events (big $|\mathrm{d}\mathbf{B}/\mathrm{dt}|$ events) in the ASC index.

5 Summary and conclusion

We developed an automatic identification scheme of sudden and significant intensification of auroral arc with expanding motion (Local-Arc-Breaking) seen in the ASC JPEG image, and applied it for real-time alert. Unlike the other automatic identification trials such as using the deep-learning neural network (none of them has so far quantified the auroral activity), the expert system in which we used a set of simple criteria and calculations successfully quantifies the auroral activity with satisfactory results in the warning purpose of the Local-Arc-Breaking. The scheme is divided into two steps: (1) obtaining a set of simple numbers that represents the sky condition of the entire ASC ($\sim 1.5\times10^5$ active pixels with a 6 byte colour information each), which we call the ASC auroral index, and (2) judging the auroral activity level only from the index values. The midterm product (ASC auroral index) is stored on real-time bases, whereas the result of activity assessment is sent as warning email real time only when the index values satisfy the Level 6 criterion. The alert system started 5 November 2021.

Table A1. Version 0.0 criterion of ASC auroral index for old ASC (Nikon D700)

classification Ver.	condition 1 classification	condition 2 H	condition 3 S	L
0.0	strong aurora:	0.20<, <0.46	0.20<, <0.8	0.20<, <0.8
0.0	green arc:	0.18<, <0.46	0.15<, <0.8	0.10≤, <0.8
0.0	visible diffuse:	0.16<, <0.50	0.10<, <0.8	0.5≤, <0.8
0.0	cloud:	< 0.16	0.10<, <0.8	0.15<, <0.8
0.1	strong aurora:	0.20≤, <0.46	0.17≤, <0.8	0.30≤, <0.83
0.1	green arc:	0.18≤, <0.46	0.13≤, <0.8	0.15≤, <0.83
0.1	visible diffuse:	0.16≤, <0.57	0.09≤, <0.8	0.5≤, <0.83
0.1	cloud:	<0.16	0.10≤, <0.8	0.15≤, <0.83
0.1	moon:		<0.13	0.75≤, ≤1

The first step is further subdivided into two stages: (1a) pixel-to-pixel classification into "strong aurora", most likely auroral arc (category "green arc"), most likely visible diffuse aurora (category "visible diffuse"), most likely "cloud", most likely "the moon", and most likely "artificial light", using just R, G, B, and H values (where H is calculated from R, G, and B values, though), and (1b) simple calculation such as the percentage of the occupying area (pixel coverage) and the characteristic intensity of the strong aurora (take nonlinear average of L and L^3 for the most luminous 4900 pixels).

The present scheme is only just version 1.0, and there is a considerable room for improvements. Nevertheless, after 5 months of the operation until the end of the 2021/2022 winter season, this algorithm successfully alerted the Local-Arc-Breaking within 10 min from when the actual brightening of aurora is detected for nearly 90Like the false positive, false negative was also very little.

The direction of the future improvement is clear, thanks to the present method with the explicit criteria and calculations: we need to upgrade the criteria at each step, based on further understanding of, for examples, the camera characteristics against different light sources and relation to the geomagnetic activities. We listed these tasks toward future improvement.

Appendix A: Version 0 classification using only HSL values

For the old KAGO's ASC (Nikon D700 camera) until April 2020, we used less accurate classification method using only HSL values only to obtain the ASC auroral index version 0 (Yamauchi et al., 2018). In this version, we just plotted the index values in our website in the real-time bases, and its archive is found at the IRF site[8]. For this real time operation, we used criterion (version 0.0) that is summarised in Table A1.

This version (version 0.0) was slightly updated for the data analyses when the operation of the old ASC (Nikon D700 camera) is finished. The revised criterion (version 0.1) is summarised in the same table.

[8]https://www.irf.se/maggraphs/aurora_detect/graphs/

Code availability. Python code is found in the supplemental material (except sending email alert part which includes private information)

Data availability. The all sky images and magnetic field data are publicly available at IRF's observatory data site https://www.irf.se/en/about-irf/data/, with ASC data at https://www.irf.se/alis/allsky/krn/, magnetic field data at https://www.irf.se/maggraphs/iaga/, and ASC auroral index at https://www.irf.se/alis/allsky/nowcast/.

Author contributions. MY is responsible all part except the calibration, maintenance and optimum setting of the ASC, for all of which UB is responsible

Competing interests. no competing interest

Acknowledgements. The work is partially funded by ESA SSA program and by the EU projectRIT (Space for innovation and growth) with the objective of developing the space region in northern Sweden. Maintenance of system including software is done by members of Kiruna Atmospheric and Geophysical Observatory (KAGO) at IRF. We also thank Dennis van Dijk for developing preliminary version (version 0) made for the old Nikon D700 camera, and Arnau Busom i Vidal for examining the Local-Arc-Breaking.

References

Akasofu, S.-I.: The development of the auroral substorm, Planet. Space Sci., 12, 273-282, DOI = 10.1016/0032-0633(64)90151-5, 1964.

Akasofu, S.-I.: Physics of magnetospheric substorms, Astrophysics and space science library, vol. 47, Reidel, Dordrecht, https://doi.org/10.1007/978-94-010-1164-8, 1977.

Brändström, B. U. E., Enell, C.-F., Widell, O., Hansson, T., Whiter, D., Mäkinen, S., Mikhaylova, D., Axelsson, K., Sigernes, F., Gulbrandsen, N., Schlatter, N. M., Gjendem, A. G., Cai, L., Reistad, J. P., Daae, M., Demissie, T. D., Andalsvik, Y. L., Roberts, O., Poluyanov, S., and Chernouss, S.: Results from the intercalibration of optical low light calibration sources 2011, Geosci. Instrum. Method. Data Syst., 1, 43?51, https://doi.org/10.5194/gi-1-43-2012, 2012.

Breiman, L.: Random Forests. Machine Learning 45, 5-32, https://doi.org/10.1023/A:1010933404324, 2001

Friis-Christensen, E., McHenry, M. A., Clauer, C. R., and Vennerstrom, S.: Ionospheric traveling convection vortices observed near the polar cleft: a triggered response to sudden changes in the solar wind, Geophys. Res. Lett., 15, 253-256, DOI = 10.1029/GL015i003p00253, 1988.

Helmholtz - German Research Centre for Geoscience (GFZ) in Potsdam, Real-time Kp, https://isdc.gfz-potsdam.de/kp-index/

Juusola, L., Vanhamäki, H., Viljanen, A., and Smirnov, M.: Induced currents due to 3D ground conductivity play a major role in the interpretation of geomagnetic variations, Ann. Geophys., 38, 983-998Ann. Geophys., 38, 983-998, DOI = https://doi.org/10.5194/angeo-38-983-2020, 2020.

Kvammen, A., Wickstrøm, K., McKay, D., and Partamies, N.: Auroral image classification with deep neural networks. J. Geophysi. Res., 125, e2020JA027808, DOI=10.1029/2020JA027808, 2020.

Liu, C., Deng, N., Wang, J.T.L. and Wang, H.: Predicting solar flares using SDO/HMI vector magnetic data products and the random forest algorithm, Astrophys. J., 843, 104, https://doi.org/10.3847/1538-4357/aa789b, 2017.

Luhr, H., Aylward, A., Bucher, S.C., Pajunpaa, A., Pajunpaa, K., Holmboe, T., and Zalewski, S.M.: Westward moving dynamic substorm features observed with the IMAGE magnetometer network and other ground-based instruments, Ann. Geophys., 16, 425-440,. DOI=10.1007/s00585-998-0425-y, 1998.

Nanjo, S., Satonori Nozawa, S., Yamamoto, M., Kawabata T., Johnsen,M.G., Tsuda, T.T, Hosokawa, K.: An a auroral detection system using deep learning: real-time operation in Tromsø, Norway, DOI=10.21203/rs.3.rs-1090985/v1, 2021.

Partamies, N., O. Amm, K. Kauristie, T. I. Pulkkinen, and E. Tanskanen, A pseudo-breakup observation: Localized currentwedge across the postmidnight auroral oval, J. Geophys. Res.,108(A1), 1020, DOI=10.1029/2002JA009276, 2003.

Sigernes, F., Holmen, S. E., Biles, D., Bjørklund, H., Chen, X., Dyrland, M., Lorentzen, D. A., Baddeley, L., Trondsen, T., Brändström, U., Trondsen, E., Lybekk, B., Moen, J., Chernouss, S., and Deehr, C. S.: Auroral all-sky camera calibration, Geosci. Instrum. Method. Data Syst., 3, 241-245, DOI=10.5194/gi-3-241-2014, 2014.

Syrjäsuo, M.T., Pulkkinen, T.I., Janhunen, P., Viljanen, A., Pellinen, R.J., Kauristie, K., Opgenoorth, H.J., Wallman, S., Eglitis, P., Karlsson, P., Amm, O., Nielsen, E., and Thomas, C.: Observationsof substorm electrodynamics using the MIRACLE network, in Substorms-4, edited by Kokubun S., and Kamide, Y.,Terra Scientific Publishing Company, Tokyo, 111-114, 1998

World data center (WDC) in Kyoto, Real-time AE, https://wdc.kugi.kyoto-u.ac.jp/ae_realtime/presentmonth/index.html

Yamauchi, M., Brandstrom, U., van Dijk, D., Sergienko, T., and Kero, J.: Improving nowcast capability through automatic processing of combined ground-based measurements, in EGU General Assembly Conference Abstracts, p. 1779, 2018.